

Contents lists available at ScienceDirect

Transportation Research Part C

journal homepage: www.elsevier.com/locate/trc





Discrete macroscopic traffic flow model considering the lane-changing behaviors in the mixed traffic environment

Yi Zhang, Xianfeng (Terry) Yang *

Department of Civil and Environmental Engineering, University of Maryland, 1173 Glenn L. Martin Hall, College Park, MD 20742, United States

ARTICLE INFO

Keywords:
Macroscopic traffic model
Lane-changing behavior
Mixed traffic flow

ABSTRACT

In the foreseeable future, the coexistence of Connected and Automated Vehicles (CAVs) and Human-Driven Vehicles (HVs) will continue to be a feature of the traffic landscape for an extended period. The accurate estimation of mixed traffic conditions becomes essential for effectively managing traffic flow and ensuring road safety. In this research, we introduce a discrete, macroscopic, and second-order traffic flow model designed to capture the complexities of the mixed traffic environment. Our approach builds upon a microscopic traffic model and considers the interactions between CAVs and HVs, as well as the distinctive driving behaviors exhibited by each vehicle type. In particular, acknowledging that CAVs behave differently from HVs, we conduct a thorough analysis of the car-following and lane-changing behaviors of HVs in the presence of CAVs. To evaluate the effectiveness of our proposed model, we carried out extensive numerical simulations on a freeway segment with variable speed controls. The simulation results highlight two key findings: First, the proposed model achieves accurate estimations of mixed traffic states, including both flow and speed parameters. Second, there is a marked improvement in performance with increasing differences in speed control between CAVs and HVs. Our research contributes to the advancement of traffic management strategies and facilitates improved traffic flow in mixed traffic conditions. Additionally, the proposed model has significant potential to aid in the design and implementation of future transportation systems that incorporate connected automated vehicles while seamlessly accommodating human-driven vehicles.

1. Introduction

Through the exchange of real-time information between vehicles and infrastructures, applications involving Connected and Automated Vehicles (CAVs) have shown promising advantages in enhancing transportation safety (Papadoulis et al., 2019) and mobility (Kavas-Torris et al., 2021). Meanwhile, CAV technology has demonstrated significant potential in mitigating traffic congestion and enhancing the efficiency of transportation systems (He et al., 2022; Peng et al., 2021; Huang et al., 2018). To capitalize on these potential benefits, numerous researchers have delved into the applications of CAV technology in various traffic control areas (Jin and Orosz, 2016; Du et al., 2020; Zhou et al., 2021). Such endeavors aid traffic agencies in effectively implementing CAV applications in real-world scenarios.

However, due to ongoing technological limitations, it is expected that CAVs will need to coexist with human-driven vehicles (HVs) and share the road network in the near future. In this mixed traffic environment, it is crucial to develop a traffic estimation

E-mail address: xtyang@umd.edu (X.T. Yang).

^{*} Corresponding author.

model that accurately captures the dynamics of CAV and HV interactions, which is essential for supporting research and applications in traffic operations (Chanut and Buisson, 2003; Bose and Ioannou, 2003; Hegyi et al., 2005; Lo and Hsu, 2010; Yang and Jin, 2014). Yet, conventional macroscopic traffic state models (Yuan et al., 2021) often fall short in reflecting the impact of controlled CAVs on the overall state of freeway traffic in most CAV applications. For instance, if CAVs are operated at a speed lower than the traffic flow under speed harmonization control, they may compel the HVs following them to either match their reduced speed or initiate lane changes to overtake.

While there is an abundance of literature on mixed traffic environments comprising both CAVs and HVs (Qin and Wang, 2019; Tajdari and Roncoli, 2021; Li et al., 2023), current models primarily focus on deriving new fundamental diagrams (Seraj et al., 2020; Guo and Ban, 2020; Zhou and Zhu, 2020; Tajdari and Roncoli, 2021; Halakoo and Yang, 2021; Shi and Li, 2021; Zhang et al., 2022) and only a few studies have concentrated on the microscopic modeling of mixed traffic dynamics, specifically by formulating a dynamic traffic model within the spatial domain (An et al., 2022). Zhang et al. (2023) is one of the first studies on the modeling of interactive gaming among multiple vehicles, introducing a tentative yet unyielding driving strategy. Wang et al. (2023) identified a negative quadratic transformation rule transitioning from the conventional temporal domain to the spatial domain, firstly presenting the longitudinal and lateral coupled planning method within the spatial domain. However, there remains a significant gap in fully capturing the intricate interactions between CAVs and HVs in the macroscopic traffic flow models. Crucial aspects such as the dynamics of CAVs operating under variable speed trajectory control, and their influence on the behavior of following HVs, remain inadequately addressed. Moreover, the relationship between sudden speed reductions in vehicles and subsequent lane-changing behavior in trailing vehicles has not been extensively explored, despite its potential significance in influencing overall traffic patterns.

In summary, the research gap in understanding mixed traffic dynamics is threefold: First, there is a pressing need for a macroscopic traffic flow model that accurately incorporates lane-changing and car-following behaviors of HVs, to provide a more comprehensive representation of CAV and HV interactions. Second, existing models (Yang et al., 2015) lack the capability to effectively manage variable speed limit (VSL) control for both CAVs and HVs in mixed traffic scenarios, a key component in optimizing traffic flow. Lastly, the influence of factors such as the penetration rate of CAVs and driver compliance rates on freeway traffic dynamics warrants further investigation to understand their roles in shaping traffic behavior in mixed environments. Addressing these critical areas is essential for advancing our understanding of mixed traffic dynamics and paving the way for more efficient and safer transportation systems that integrate CAVs and HVs seamlessly.

This study addresses the highlighted challenges by introducing a novel second-order, multi-class macroscopic traffic state model, adept at capturing the complex dynamics between CAVs and HVs as distinct entities. This model, emerging from an extensive kinematic analysis of both vehicle types, effectively overcomes the limitations inherent in existing methodologies. We have developed this macroscopic model based on its microscopic counterpart, integrating critical aspects such as the lane-changing behavior of HV drivers and their responses to variable speed limit (VSL) controls. This integration not only enhances the model's realism but also ensures a more faithful representation of real-world mixed traffic conditions. By distinctly categorizing CAVs and HVs within the model, it facilitates a deeper understanding of their unique driving behaviors and their subsequent impact on traffic dynamics. The multi-class nature of the model is particularly beneficial, allowing for an in-depth study of the behavior patterns of CAVs and HVs separately. Such an approach provides a holistic understanding of their interactions and their collective influence on traffic flow, offering valuable insights for the development of more efficient and safer transportation systems.

The following sections of this paper are structured as: Literature review is conducted in Section 2. Then, Section 3 presents the methodology based on kinematic analysis and mathematics modeling. Section 4 describes the design of numerical experiment, followed by the discussion on the effectiveness of the traffic model proposed in this research in Section 5. Lastly, the conclusion is presented in the final section.

2. Literature review

Scholars have devoted considerable time and effort to the examination of mixed traffic flow models over a long time. The nascent mixed traffic flow models that emerged in the early stages of research were originally formulated for general vehicular systems, with a primary emphasis on the car-following kinematic theory. Subsequently, macroscopic models were developed by drawing inspiration from physical paradigms, exemplified by the utilization of the kinematic wave model (Zhang and Jin, 2002) and the anisotropic continuum model (Tang et al., 2007). Simultaneously, with a focus on extant traffic elements, scholars have introduced traffic models tailored to diverse mixed traffic scenarios, such as mixed buses and cars system (Koshy and Arasan, 2005; Yang et al., 2012), auto-rickshaws and heavy vehicles system (Asaithambi et al., 2018), motorized vehicles and non-motorized vehicles system (Hu et al., 2012), and motorcycles and cars system (Meng et al., 2007).

The burgeoning advancements in information technology have incited a pronounced upswing in scholarly attention devoted to the field of automated transportation systems. Nevertheless, due to inherent technological constraints, the realization of a fully autonomous environment remains a protracted endeavor. Consequently, the imminent cohabitation of automated vehicles and HVs is anticipated. As a result, researchers have progressively redirected their scholarly endeavors toward the development of traffic models tailored to address the intricate dynamics inherent in a heterogeneous automated traffic system (Yuan et al., 2009; Ngoduy et al., 2009; Guo et al., 2021).

In order to address the issue of traffic flow modeling within a heterogeneous automated environment, scholars commenced their investigations by focusing on the context of the ACC-HV mixed environment (Yuan et al., 2009; Ngoduy et al., 2009). Then, researchers switched to developing models for the AV-HV mixed traffic environment. With an emphasis on addressing this issue at the link level, Levin and Boyles (2016) initiated the development of this field by introducing a multi-class cell transmission model

Table 1
List of mixed traffic flow model.

Research	rch Vehicle type Model		Scope	LC	
Zhang and Jin (2002)	HVs	Kinematic Wave Model	Macro	No	
Tang et al. (2007)	HVs	Anisotropic Continuum Model	Macro	No	
Zhao et al. (2022)	HVs	Comfortable Driving Model	Micro	2 lanes	
Yuan et al. (2009)	ACC Vehicles and HVs	Cellular Automaton, Constant Time Headway	Micro	No	
Ngoduy et al. (2009)	ACC Vehicles and HVs	Multi-class Gas-kinetic Theory	Macro	No	
Levin and Boyles (2016)	AVs and HVs	Multiclass Cell Transmission	Link-level	No	
Wang et al. (2017)	AVs and HVs	Second-order Cell Transmission	Macro	No	
Zhu and Zhang (2018)	AVs and HVs	Bando's Model	Micro	No	
Zheng et al. (2020)	AVs and HVs	Newell's Model	Micro	No	
Shi and Li (2021)	AVs and HVs	Fundamental Diagram	Macro	No	
Guo et al. (2023)	AVs and HVs	Cellular Automata	Micro	No	
Zhang et al. (2018)	CAVs and HVs	Virtual Internal-External Forces	Macro	No	
Yao et al. (2019)	CAVs and HVs	Fundamental Diagram	Macro	No	
Zhou and Zhu (2020)	CAVs and HVs	Fundamental Diagram	Macro	No	
Lu et al. (2020)	CAVs and HVs	Generalized Additive Model (GAM)	Macro	No	
Guo et al. (2021)	CAVs and HVs	Link Transmission Model	Link-level	No	
Yao et al. (2022)	CAVs and HVs	Fundamental Diagram	Macro	No	
Wang and Wu (2023)	CAVs and HVs	Fundamental Diagram	Macro	No	
Ma et al. (2023)	CAVs and HVs	Intelligent Driver Model	Micro	No	
Li et al. (2023)	CAVs and HVs	Cellular Automata	Micro	2 lanes	
Yao et al. (2023)	CAVs and HVs	Markov Chain	Micro	No	

designed for road networks shared by human-driven vehicles and autonomous vehicles. The cell transmission model was also used by Wang et al. (2017) to develop a second-order macroscopic traffic flow model for AV-HV mixed environment. In addition to link-level and macroscopic models, researchers have also developed microscopic models (Zhu and Zhang, 2018; Zheng et al., 2020; Guo et al., 2023) and fundamental diagram models (Shi and Li, 2021).

In recent years, scholarly investigations have directed their focus toward the modeling of mixed CAV-HV environments. The majority of these research endeavors predominantly undertake the development of microscopic-scale models, as evidenced by the works of Ma et al. (2023), Li et al. (2023), and Yao et al. (2023), among others. Furthermore, some scholars have delved into link-level modeling (Guo et al., 2021), while others have advanced the field through the proposal of macroscopic traffic flow models (Zhang et al., 2018) as well as fundamental diagram models (Yao et al., 2019; Zhou and Zhu, 2020; Lu et al., 2020; Yao et al., 2022; Wang and Wu, 2023).

Additionally, scholars have observed that lane-changing behaviors exert a discernible influence on the dynamics of traffic flow. The lane-changing behaviors exhibited by motorcycles (Meng et al., 2007), and non-motorized vehicles (Hu et al., 2012), possess the potential to exert an influence on the driving dynamics of automobiles. The proposed microscopic mixed traffic flow models, which take into account lane-changing behaviors, have been proposed for mixed-length vehicle environments (Zhao et al., 2022) and mixed CAV-HV environments (Li et al., 2023) (see Table 1).

In summary, the researchers have addressed the mixed traffic flow modeling problem by meticulous consideration of the distinctive characteristics inherent to each category of vehicular entities. The extant CAV-HV mixed traffic models presently available in the literature predominantly emanate from microscopic car-following models. These models expound upon the distinctive behaviors exhibited by CAVs and HVs, while making the simplifying assumption of no lane-changing within the system. Only a limited number of recent studies have incorporated lane-changing behaviors into their investigations. Furthermore, among the mixed traffic flow models that have addressed lane-changing behaviors, the predominant focus has been on microscopic models, with researchers typically restricting their analysis to lane-changing behaviors involving only two lanes, as opposed to encompassing multiple lanes.

The primary research objective addressed within the scope of this paper is the formulation and development of a macroscopic traffic flow model specifically tailored to mixed environments accommodating both CAVs and HVs. This model endeavors to account for the intricate dynamics associated with car-following behaviors and lane-changing behaviors in multi-lane roadways, where the number of lanes exceeds or is equal to three.

3. Problem statement

In this paper, the scenario we want to focus on is a multi-lane highway with a mixed-traffic environment, and two types of vehicles coexist: CAVs and HVs. The speed control information, VSL, is posted on the roadside variable message boards for human drivers in HVs and dispatched from the central system for CAVs. The acceleration and speed of vehicles are affected by the VSL control and the moving of surrounding vehicles. Human drivers are capable of changing lanes to adjacent lanes in the mixed-traffic environment (see Fig. 1).

When the VSL control is triggered, the CAV will strictly follow the VSL control, while the HVs have more random and complicated behaviors because they are controlled by humans. Even though the VSLs are posted and most drivers would obey the speed limit (Compliant Human-driven Vehicles, CHVs), it is also possible that some drivers would not follow the control speed and have a higher

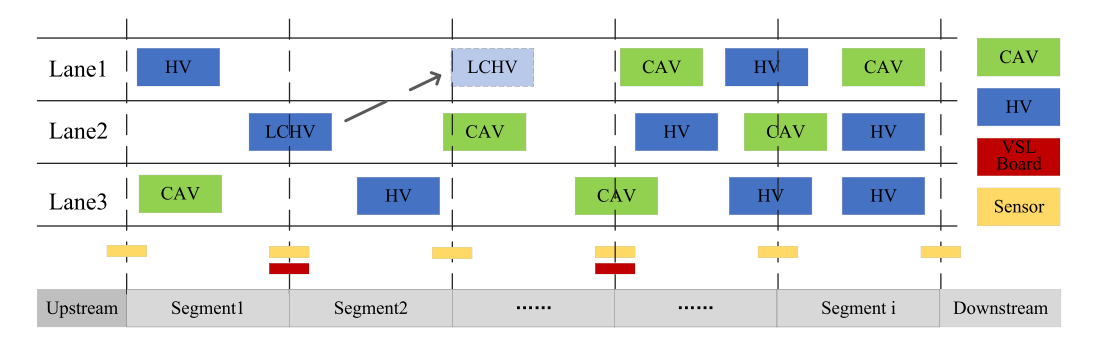


Fig. 1. The CAV-HV mixed traffic environment with VSL.

desire speed (Uncompliant Human-driven Vehicles, UHVs). Besides that, being surrounded and pushed by speed-decreased vehicles, some HV drivers could change lanes to adjacent lanes if possible (Lane-changing Human-driven Vehicles, LCHV). In summary, there are 4 classes of vehicles including CAV, CHV, UHV, and LCHV in the mixed-traffic environment.

This paper aims to propose a discrete macroscopic traffic model to estimate the traffic status in the mixed traffic environment. Based on the current traffic flow status information including current speed, density, CAV penetration rate, etc., the proposed model shall accurately estimate the traffic flow status in each highway segment for the next time interval.

3.1. Assumptions

To build model for a general mixed traffic flow environment, following assumptions are considered:

- 1. The road geometry will not affect the driver's behavior and vehicle movement.
- 2. The weather condition is assumed to be fine and will not affect the driver's behaviors and vehicle movements.
- 3. The driver's characteristics and personalities are the same and will not affect the driver's behavior and vehicle movement.
- 4. Different vehicles (CAV, Compliant HV, Uncompliant HV, Lane-changing HV) are evenly distributed on the road.
- 5. Vehicles of the same type have the same movement criteria and will not affect the driver's behavior and vehicle movement.
- 6. The human drivers are greedy, if the lane-changing conditions are satisfied, they will change the lane.

3.2. Notifications

The notifications used in this paper are listed in Table 2.

4. Model formulation

In this section, we aim to estimate the traffic status in a mixed traffic environment governed by variable speed limit control. To achieve this, we propose a discrete macroscopic model, which is developed through a detailed analysis of each vehicle category. This model originates from a microscopic perspective, incorporating both car-following and lane-changing models to describe the movement of different classes of vehicles. The macroscopic model is then formulated by extrapolating the microscopic behaviors of each vehicle class, providing a more comprehensive view of the traffic dynamics. Finally, we introduce a second-order discrete macroscopic traffic model specifically tailored for highway segments. This model integrates the behaviors of individual component vehicles, thus offering a nuanced and accurate representation of mixed traffic conditions on highways (see Fig. 2).

4.1. Microscopic models

4.1.1. Car-following behavior

The car-following behavior could be described by microscopic car-following models. Based on the full velocity difference model (FVDM, Jiang et al. (2001)), the car-following acceleration function over time for vehicles with VSL could be described as:

$$\dot{v}_m(t) = \frac{V^{opt}(s(t)) - v_m(t)}{\tau} - \gamma(v_m(t) - v_{m+1}(t)) \tag{1}$$

$$\dot{v}_{m}(t) = \frac{V^{opt}(s(t)) - v_{m}(t)}{\tau} - \gamma(v_{m}(t) - v_{m+1}(t)) \tag{1}$$

$$V^{opt} = \begin{cases} V^{VSL} & \text{Under Control} \\ V^{free} & \text{Otherwise} \end{cases}$$

When a vehicle is unaffected by Variable Speed Limits (VSL), its optimal speed function, denoted as Vopt, corresponds to the free-flow speed. However, when the vehicle enters a VSL-controlled area, Vopt adjusts to match the VSL speed designated for that specific road segment. Although the car-following model functions remain consistent across CHVs, CAVs, and UHVs, the distinct

Table 2
Notifications used in this paper.

Notification	Meaning
veh	Vehicle type set in this system, $\{1 = CAV, 2 = CHV, 3 = UHV, 4 = LCHV\}$
CFV	Vehicle type set of car-following vehicles in this system, $\{1 = CAV, 2 = CHV, 3 = UHV\}$
I	Road segment set, $I = \{1, 2, \dots, i, \dots\}$
J	Lane number set, $J = \{1, 2,, j,\}$
K	Time interval set, $K = \{1, 2, \dots, k, \dots\}$
M	Vehicle sequence set, $M = \{1, 2, \dots, m, \dots\}$
$P_{i,j}(k)$	Vehicle proportion matrix for road segment i and lane j at time interval k , $P_{i,j}(k) = [P_{i,j}^{CAV}(k), P_{i,j}^{CHV}(k), P_{i,j}^{LHV}(k), P_{i,j}^{LCHV}(k)]$
$V_{i,j}(k)$	Vehicle velocity matrix for road segment i and lane j at time interval k , $V_{i,j}(k) = [V_{i,j}^{CAV}(k), V_{i,j}^{CHV}(k), V_{i,j}^{ULHV}(k), V_{i,j}^{ULHV}(k)]$
$v_{i,j}(k)$	Traffic speed for road segment i and lane j at time interval k
$d_{i,j}(k)$	Traffic density for road segment i and lane j at time interval k
$q_{i,j}(k)$	Traffic flow for road segment i and lane j at time interval k
ΔT	The discrete time interval
$\dot{v}(t)$	The acceleration function over time
	The acceleration function over time The acceleration function of LCHV following a N-vehicle platoon
$\dot{v}_{LCHV}(t, N)$ $v(t)$	The speed function over time
V^{opt}	
•	The optimal velocity function
τ	Sensitivity for speed differences between current speed and optimal velocity
γ V free	Sensitivity for speed differences between current speed and leading vehicle's speed
•	The optimal velocity function with free flow speed as desired speed
V ^{VSL}	The optimal velocity function with VSL speed as desired speed
S_{safe}	Lane-changing safe distance
S_{adv}	Lane-changing advantage distance
s_0	The minimum acceptable following distance
S_f	The car-following distance on the current lane
T	The steady-state time gap
Δa	The lane-changing threshold acceleration
a_{bias}	The asymmetry term related to driver's lane-changing preference
b_{safe}	The safe deceleration for drivers
v_{LC}	The speed of the lane-changing vehicle
v_l	The speed of the leading vehicle in the current lane
v _f	The speed of following vehicle on the target lane
v _î	The speed of leading vehicle on the target lane
τ_i	Sensitivity for speed differences between current speed and optimal velocity
$\stackrel{\iota}{L}_{i}$	Sensitivity for speed differences between current speed and optimal velocity
opt v _{i,j}	Optimal speed for vehicles on road segment <i>i</i> and lane <i>j</i>
$v_{i,j}^{VSL}$ $v_{i,j}^{free}$	VSL speed on road segment <i>i</i> and lane <i>j</i>
of ree	Free flow speed on road segment i and lane j
$a_{i,j}$	The speed exponent term of segment i and lane j
$\alpha_{i,j}(k)$	The CAV penetration rate on road segment i and lane j at time interval k
$\beta_{i,j}(k)$	The CHV rate on road segment i and lane j at time interval k
	The parameters in the dynamic speed equations of segment <i>i</i>
v _i	The number of LCHV from lane j to $j+1$ on road segment i
$n_{i,j,j+1}$	The LCHV rate from lane j to $j+1$ on road segment i at time interval k
$\omega_{i,j,j+1}(k)$	
9 oinitial	The proportion of VSL-compliant vehicles
s ^{initial}	The car-following distance before lane-changing on lane <i>j</i> .
S final S j	The car-following distance after lane-changing on lane <i>j</i>
$S_{j,j+1}^{initial}$	The minimum threshold car-following distance on lane $j + 1$ for vehicles could change lanes from lane j
$S_{j,j+1}^{final}$	The maximum threshold car-following distance on lane $j + 1$ for vehicles could not change lanes from lane

behaviors in car-following among these categories can be delineated accordingly due to the varied desired speeds among them. For CHVs and CAVs, their V^{opt} transitions to V^{VSL} upon entering an activated VSL area, whereas for UHVs, V^{opt} remains constant regardless of the area traversed.

4.1.2. Lane-changing behavior

In the context of FVDM, there are generally two conditions under which lane-changing occurs (Treiber and Kesting, 2013). Fig. 3 depicts the decision-making process that human drivers undergo when considering a lane change. When both of these lane-changing conditions are met, an HV may decide to change lanes in order to maintain or achieve a higher driving speed.

The lane-changing conditions could be described as:

1. The distance between the new following vehicle on the target lane should be larger than the safe distance.

$$S_{safe} = s_0 + T \left[v_{\hat{f}} - \tau b_{safe} + \gamma \tau (v_{\hat{f}} - v_{LC}) \right]$$
(3)

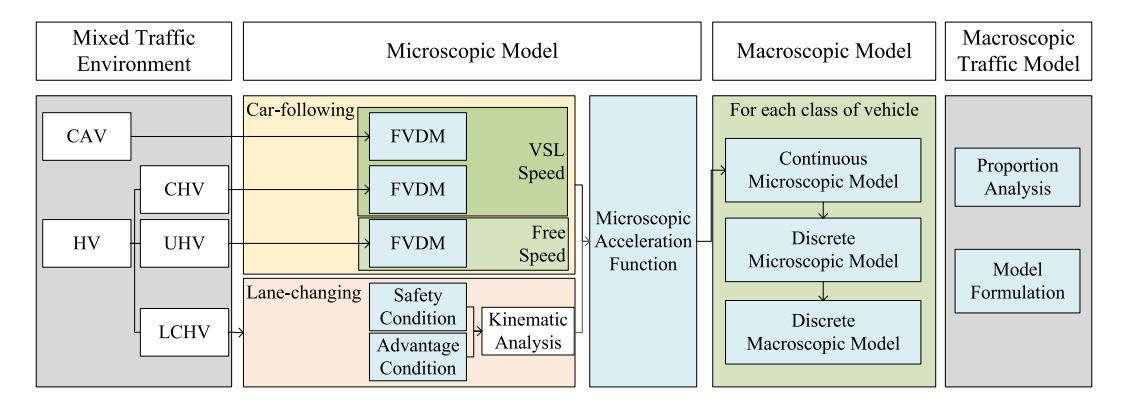


Fig. 2. Model structure.

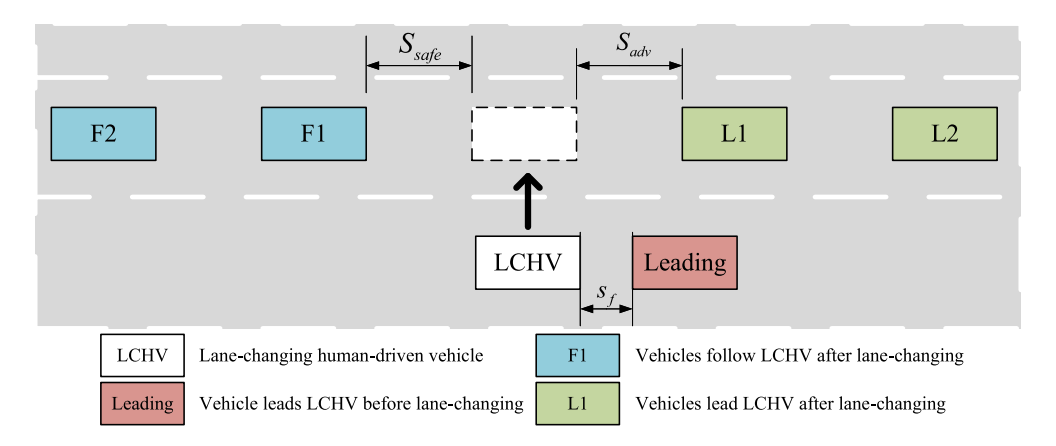


Fig. 3. Lane-changing scenario for LCHV.

2. The distance between the new previous vehicle on the target lane should be larger than the advantage distance.

$$S_{adv} = s_f + T\tau[\Delta a + a_{bias} + \gamma(v_l - v_{\hat{l}})] \tag{4}$$

4.2. Macroscopic models for different vehicles

In accordance with the discussion in Section 3, the mixed traffic environment comprises four distinct classes of vehicles, including CAV, CHV, UHV, and LCHV. When there is no VSL control implemented on a particular road segment, all vehicles will operate at the free flow speed, which is considered the optimal velocity under those conditions.

However, when the VSL system is activated, specifically when CAVs and CHVs are passing through the controlled segments, their optimal velocities will be adjusted to match the prescribed VSL speed. In contrast, the optimal velocities of UHVs and LCHVs will remain at the free flow speed. This is because the drivers of these vehicle classes typically prefer to maintain a higher speed, even when VSL control is in effect.

4.2.1. Macroscopic model for car-following vehicles

The macroscopic discrete velocity function of each category of car-following vehicles in road segment i and lane j at time interval k+1 could be derived based on the microscopic function.

From FVDM, the car following function could be written as Eq. (5).

$$\dot{v}_i(t) = \frac{V^{opt}(s(t)) - v_i(t)}{\tau} - \gamma(v_i(t) - v_{i+1}(t)) \tag{5}$$

Then, the velocity function in discrete time ΔT could be written as:

$$v_i(t + \Delta T) - v_i(t) = \frac{\Delta T}{\tau} \left[V^{opt}(d(t)) - v_i(t) \right] - \Delta T \gamma \left[v_i(t) - v_{i+1}(t) \right] \tag{6}$$

When the traffic flow is under an equilibrium condition, all vehicles in segment i has the same velocity, so, the speed function for road segment i and lane j at time interval k + 1 could be written as:

$$v_{i,j}(k+1) = v_{i,j}(k) + \frac{\Delta T}{2} \left[V^{opt}(d(k)) - v_{i,j}(k) \right] - \Delta T \gamma \left[v_{i,j}(k) - v_{i+1,j}(k) \right]$$
(7)

Considering the impact of traffic density on the traffic speed, we could get the model for road segment i and lane j at time interval k + 1, which is the METANET model (Messmer and Papageorgiou, 1990) speed function.

$$v_{i,j}^{CFV}(k+1) = v_{i,j}^{CFV}(k) + \frac{\Delta T}{\tau_i} \left[V_{i,j}^{veh}(d_{i,j}(k)) - v_{i,j}^{CFV}(k) \right] + \frac{v_{i,j}^{CFV}(k)\Delta T}{L_i} \left[v_{i-1,j}^{CFV}(k) - v_{i,j}^{CFV}(k) \right] - \frac{v_i \Delta T}{\tau_i L_i} \frac{[d_{i+1,j}(k) - d_{i,j}(k)]}{[d_{i,j}(k)]}$$
(8)

$$V_{i,j}^{veh}(d_{i,j}(k)) = v_{i,j}^{opt} exp \left[-\frac{1}{a_{i,i}} \left(\frac{d_{i,j}(k)}{d_{cr}} \right)^{a_{i,j}} \right]$$
(9)

METANET is a widely used second-order discrete macroscopic traffic model. It has been used to describe the multi-class traffic situation (Liu et al., 2014, 2016).

In Eq. (8), k denotes the time step presently in the calculation. $d_{i,j}(k)$ denotes traffic density for road segment i and lane j at time interval k, $v_{i,j}^{CFV}$ denotes traffic speed for road segment i and lane j for car-following vehicles belonging to CFV set. ΔT is the macroscopic simulation time step, and L_i denotes the length of road segment i. $V_{i,j}^{veh}$ represents the fundamental diagram function for vehicles within the CFV set, encompassing CAVs, CHVs, and UHVs. This function, denoted as Eq. (9), was introduced by Messmer and Papageorgiou (1990).

The primary distinction among CHVs, CAVs, and UHVs lies in their car-following behaviors, specifically in their adherence to required speeds, a difference reflected in the varying desired velocities outlined in Eq. (10) and Eq. (11).

For CHVs and CAVs, V^{opt} transitions to V^{VSL} upon entering an activated VSL area:

$$v_{i,j}^{opt} = \begin{cases} v_{i,j}^{VSL} & \text{Under VSL Control} \\ v_{i,i}^{free} & \text{Otherwise} \end{cases}$$
 (10)

For UHVs, Vopt remains constant regardless of the area traversed:

$$v_{i,j}^{opt} = v_{i,j}^{free} \tag{11}$$

4.2.2. Macroscopic model for lane-changing human-driven vehicles

Microscopic lane-changing behaviors could also affect the macroscopic traffic flow status (Laval and Leclercq, 2008; Jin, 2010; Rahman et al., 2013). Thus, it is necessary to analyze the dynamic of lane-changing vehicles in the mixed-traffic environment.

In the discrete macroscopic traffic flow model, the time period is generally set as 10–15 min (Kotsialos et al., 2002), in which the maneuver of lane-changing human-driven vehicles (LCHVs) could be divided into two parts: lane-changing and carfollowing after lane-changing. The insignificance of lane-changing's short-term impact is apparent, given that it consumes a mere 1–2 s (Ahmed, 1999), in stark contrast to the considerably lengthier temporal interval spanning 10–15 min. Consequently, this research predominantly directs its attention toward the car-following behavior of LCHV subsequent to lane-changing.

Following the lane-changing maneuver, the LCHV will proceed to trial and establish alignment behind the leading vehicles within the target lane. These leading vehicles encompass both VSL-compliant vehicles, including CAVs and CHVs, as well as VSL-uncompliant vehicles, denoted as UHVs. The subsequent car-following behavior of LCHV on the target lane is contingent upon the behavior of the vehicles it follows.

When the VSL control is activated, vehicles that obey the VSL, including CAVs and CHVs, will adjust their optimal speed to adhere to the prescribed VSL speed. Consequently, this adjustment leads to a gradual reduction in their velocity as they pass a designated VSL control zone. When the VSL is triggered in the equilibrium status, the velocity of VSL-compliant vehicles is either equivalent to that of their preceding vehicle, provided it is a CAV or CHV, or lower, in the event their preceding vehicle is a UHV. Then, the optimal velocity model (OVM, Bando et al. (1995)) may aptly characterize their car-following behaviors, as speed differences exert negligible influence on their acceleration function.

$$\dot{v}_m(t) = \frac{V^{VSL}(s(t)) - v_m(t)}{}$$
(12)

For VSL-uncompliant vehicles, their optimal speed remains unaffected by the lower VSL speed. Nonetheless, if the preceding vehicle reduces its speed, the non-compliant VSL vehicle will experience a deceleration due to the widening speed differential. This dynamic can be expressed through an acceleration function as follows:

$$\dot{v}_m(t) = \frac{V^{free}(s(t)) - v_m(t)}{\tau} - \gamma (v_m(t) - v_{m+1}(t)) \tag{13}$$

With the VSL control, The distance between the VSL-compliant vehicle and the preceding vehicle will progressively increase after it approaches a VSL control spot, while the car-following distance of the VSL-uncompliant vehicle will not increase. As a result, the VSL-compliant vehicle can be considered the leader of a platoon, consisting of several UHVs that desire a higher speed but are also influenced by the deceleration of the VSL-affected vehicle, along with the LCHV itself.

Lemma 1: (Proved in Appendix B.1) In a given road segment, a higher proportion of VSL-affected vehicles leads to a shorter platoon length. **Lemma 2**: (Proved in Appendix B.2) The further a CAV or a CHV is from the LCHV, the later the LCHV will decelerate its speed.

Considering the influence of the ratio of VSL-compliant vehicles, the car-following model of LCHV could be derived. If there are *N* vehicles before the LCHV, the first vehicle is a VSL-compliant vehicle, and the other following vehicles are UHVs (see Fig. 4).

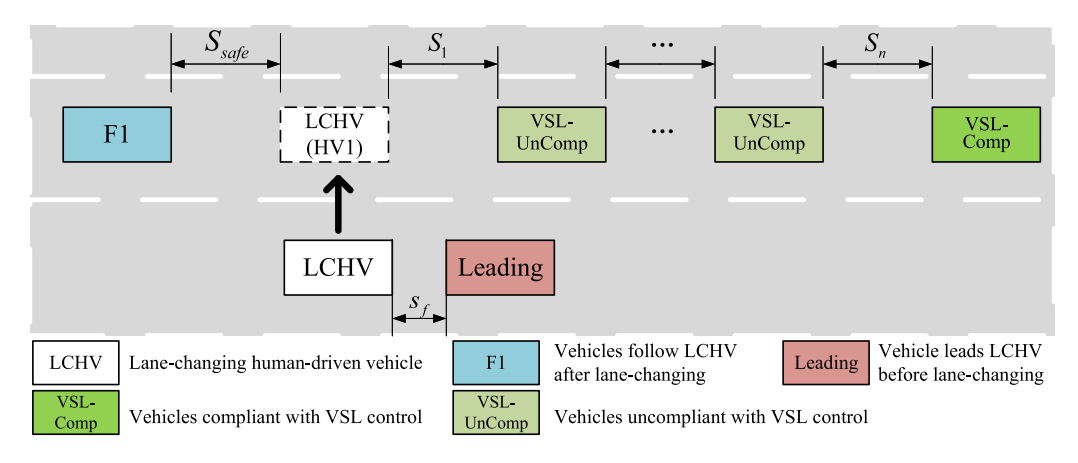


Fig. 4. LCHV following N-vehicle platoon after lane-changing

Theorem 1 (Proved in Appendix C).: The car-following acceleration function of the LCHV following a N vehicle platoon after the lane-changing is:

$$\dot{v}_{LCHV}(t,N) = \sum_{n=1}^{N} \left[\frac{\Delta t}{L}^{n-1} \left(\frac{V(s_n(t)) - v_n(t)}{\tau} - \frac{v_n(t)(v_n(t) - v_{n+1}(t))}{L} \right) \prod_{n=1}^{N-1} v_n(t) \right]$$
(14)

The penetration rate of CAVs is α on a freeway segment, and the proportion of CHVs is β , thus, the proportion of VSL-compliant vehicles in the traffic flow is $\theta = \alpha + \beta$. Therefore, the probability of following an N-vehicle platoon is $\theta(1-\theta)^{N-1}$. Generally, by summarizing all possible situations together, the acceleration function for the LCHV is Eq. (15):

$$\dot{v}_{LCHV}(t) = \sum_{N=1}^{\infty} \theta (1 - \theta)^{N-1} \sum_{n=1}^{N} \left(\left(\frac{\Delta t}{L} \right)^{n-1} \left(\frac{V(t) - v_n(t)}{\tau} - \frac{v_n(t)(v_n(t) - v_{n+1}(t))}{L} \right) \prod_{n=1}^{N-1} v_n(t) \right)$$
(15)

This equation exhibits convergence. Because as N goes to infinity, $\theta(1-\theta)^{N-1}$ converges to 0. Then, the summary of $\theta(1-\theta)^{N-1}v_{ICHV}(t,N)$ converges to a certain value.

Having the acceleration function and considering the density as Section 4.2.1, the discrete macroscopic traffic flow model of LCHV in road segment i and lane j at time interval k + 1 could be written as:

$$v_{i,j}^{LCHV}(k+1) = \Delta T \left[\sum_{N=1}^{\infty} \theta_{i,j}(k) (1 - \theta_{i,j}(k))^{N-1} \sum_{n=1}^{N} \left(\left(\frac{\Delta t}{L_i} \right)^{n-1} \left(\frac{V(d_{i,j}(k)) - v_{i,j}(k)}{\tau_i} + \frac{v_{i,j}(k)(v_{i-1,j}(k) - v_{i,j}^{LCHV}(k))}{L_i} \right) \prod_{n=1}^{N-1} v_n(k) \right] + v_{i,j}^{LCHV}(k) - \frac{v_i \Delta T}{\tau_i L_i} \left[\frac{d_{i+1,j}(k) - d_{i,j}(k)}{d_{i,j}(k)} \right]$$
(16)

4.3. Discrete macroscopic multi-class traffic model

4.3.1. Ratio analysis

In the mixed traffic environment, the proportion of each category of vehicle could also impact the traffic flow estimation. The penetration rate shows the proportion of CAV, while β shows the proportion of CHVs. The proportion of LCHVs should still be analyzed.

For two adjacent lanes, the number of lane-changing vehicles could be calculated based on traffic status (density, speed) and lane-changing conditions (Proved in Appendix A). However, for the multi-lane scenario, the relation of lanes should still be considered.

For the multi-lane scenario, the inner lanes have two adjacent lanes. When calculating the number of lane-changing vehicles between an inner lane j and one of its adjacent lanes j-1, the lane-changing between the inner lane j and another adjacent lane j+1 could also change the traffic status on the middle lane j. Therefore, for inner lanes, the real lane-changing volume should be adjusted from the initial lane-changing volume $n_{i,j,j+1}$ and $n_{i,j,j-1}$. For segment i on a three-lane highway, the adjustment of middle lanes should be conducted as:

 $n_{i,j,j+1}$ represents the number of lane-changing vehicles from lane j to j+1 on segment i. If $n_{i,j,j+1} > 0$, vehicles in lane j move to lane j+1, while if $n_{i,j,j+1} < 0$, vehicles in lane j+1 move to lane j.

If $n_{i,j,j+1} > 0$ and $n_{i,j,j-1} > 0$, or $n_{i,j,j+1} < 0$ and $n_{i,j,j-1} < 0$, the adjustment should be conducted as:

$$n_{1_{\min\{|n_{i,j,j+1}|,|n_{i,j,j-1}|\}}} = \frac{\min\{|n_{i,j,j+1}|,|n_{i,j,j-1}|\}}{n_{i,j,j+1} + n_{i,j,j-1}} \cdot \min\{|n_{i,j,j+1}|,|n_{i,j,j-1}|\}$$
(17)

$$n_{1_{\max\{|n_{i,j,j+1}|,|n_{i,j,j-1}|\}}} = \frac{\max\{|n_{i,j,j+1}|,|n_{i,j,j-1}|\}}{n_{i,j,j+1} + n_{i,j,j-1}} \cdot \min\{|n_{i,j,j+1}|,|n_{i,j,j-1}|\} + \max\{|n_{i,i,j+1}|,|n_{i,i,j-1}|\} - \min\{|n_{i,i,j+1}|,|n_{i,i,j-1}|\}$$

$$(18)$$

Then, the proportion of the lane-changing vehicle from lane j to j + 1 on segment i in time interval k could be written as:

$$\omega_{i,j,j+1}(k) = \frac{n_{i,j,j+1}(k)}{n_{i,i}(k)} \tag{19}$$

The proportion of the UHV in lane j on segment i in time interval k could be written as:

$$P_{i,j}^{UHV}(k) = 1 - \alpha_{i,j}(k) - \beta_{i,j}(k) - \omega_{i,j,j+1}(k) - \omega_{i,j,j-1}(k)$$
(20)

Thus, the final proportion matrix $P_{i,j}(k)$ of each class of vehicle on segment i lane j in time interval k could be written as:

$$P_{i,j}(k) = \left[P_{i,j}^{CAV}(k), P_{i,j}^{CHV}(k), P_{i,j}^{UHV}(k), P_{i,j}^{LCHV}(k) \right]$$

$$= \left[\alpha_{i,j}(k), \quad \beta_{i,j}(k), \quad 1 - \alpha_{i,j}(k) - \beta_{i,j}(k) - \omega_{i,i,j+1}(k) - \omega_{i,i,j-1}(k), \quad \omega_{i,i,j+1}(k) + \omega_{i,i,j-1}(k) \right]$$
(21)

4.3.2. Discrete macroscopic multi-class traffic model

Based on the kinematic analysis of CAVs, CHVs, UHVs, and LCHVs in Section 4, the second-order multi-class discrete macroscopic traffic flow model proposed in this research could be summarized as follows:

The speed function for lane j on segment i in time interval k + 1, $v_{i,j}(k + 1)$, could be written as the summary of the products of vehicle proportion and speed for each class.

$$v_{i,j}(k+1) = P_{i,j}(k)V_{i,j}(k+1)^{\mathsf{T}}$$
 (22)

where the proportion matrix $P_{i,j}(k)$ and the speed matrix $V_{i,j}(k+1)$ be written as:

$$P_{i,j}(k) = \begin{bmatrix} \alpha_{i,j}(k), & \beta_{i,j}(k), & 1 - \alpha_{i,j}(k) - \beta_{i,j}(k) - \omega_{i,i,j+1}(k) - \omega_{i,j,j-1}(k), & \omega_{i,j,j+1}(k) + \omega_{i,j,j-1}(k) \end{bmatrix}$$
(23)

$$V_{i,i}(k+1) = [v_{i,i}^{1}(k+1), v_{i,i}^{2}(k+1), v_{i,i}^{3}(k+1), v_{i,i}^{4}(k+1)]$$
(24)

The speed function of each class of car-following vehicles, the Eq. (25) describes vehicles in set $CHV = \{1, 2, 3\}$, and Eq. (26) describes LCHVs. Accordingly, the optimal velocity function is formulated as Eq. (27) and Eq. (28).

$$v_{i,j}^{CFV}(k+1) = v_{i,j}^{CFV}(k) + \frac{\Delta T}{\tau_i} \left[V_{i,j}^{CFV}(d_{i,j}(k)) - v_{i,j}^{CFV}(k) \right] + \frac{v_{i,j}^{CFV}(k)\Delta T}{L_i} \left[v_{i-1,j}^{CFV}(k) - v_{i,j}^{CFV}(k) \right] - \frac{v_i \Delta T}{\tau_i L_i} \frac{[d_{i+1,j}(k) - d_{i,j}(k)]}{[d_{i,j}(k)]}$$
(25)

$$v_{i,j}^{LCHV}(k+1) = v_{i,j}^{LCHV}(k) - \frac{v_i \Delta T}{\tau_i L_i} \left[\frac{d_{i+1,j}(k) - d_{i,j}(k)}{d_{i,j}(k)} \right] +$$

$$\Delta T \left[\sum_{N=1}^{\infty} \alpha_{i,j}(k) (1 - \alpha_{i,j}(k))^{N-1} \sum_{n=1}^{N} \left(\left(\frac{\Delta t}{L_i} \right)^{n-1} \left(\frac{V(d_{i,j}(k)) - v_{i,j}(k)}{\tau_i} + \frac{v_{i,j}(k) (v_{i-1,j}(k) - v_{i,j}^{LCHV}(k))}{L_i} \right) \prod_{n=1}^{N-1} v_{i,j}(k) \right) \right]$$
(26)

$$V_{i,j}^{veh}(d_{i,j}(k)) = v_{i,j}^{opt} exp\left[-\frac{1}{a_{i,i}} \left(\frac{d_{i,j}(k)}{d_{cr}} \right)^{a_{i,j}} \right]$$
 (27)

$$v_{i,j}^{opt} = \begin{cases} = \begin{cases} v_{i,j}^{VSL} & \text{Under VSL Control} \\ v_{i,j}^{free} & \text{Otherwise} \end{cases} & \text{Vehicle Type is 1 or 2} \end{cases}$$

$$= v_{i,j}^{free} & \text{Vehicle Type is 3 or 4}$$
(28)

Then, the overall density is the summary of CAV density and HV density, and the overall flow is the summary of CAV flow and HV flow.

$$d_{i,j}(k) = d_{i,j}^{\text{CAV}}(k) + d_{i,j}^{\text{HV}}(k)$$
(29)

$$d_{i,j}^{\text{CAV}}(k+1) = d_{i,j}^{\text{CAV}}(k) + \frac{\Delta T}{L_i} \left[q_{i-1,j}^{CAV}(k) - q_{i,j}^{CAV}(k) + r_{i,j}^{CAV}(k) - s_{i,j}^{CAV}(k) \right]$$
(30)

$$d_{i,j}^{\mathrm{HV}}(k+1) = d_{i,j}^{\mathrm{HV}}(k) + \frac{\Delta T}{L_i} \left[q_{i-1,j}^{HV}(k) - q_{i,j}^{HV}(k) + r_{i,j}^{HV}(k) - s_{i,j}^{HV}(k) \right] - \frac{n_{i,j,j-1}(k) + n_{i,j,j+1}(k)}{L_i} \tag{31}$$

$$q_{i,j}(k) = q_{i,j}^{\text{CAV}}(k) + q_{i,j}^{\text{HV}}(k)$$
 (32)

$$q_{i,j}(k) = d_{i,j}^{\text{veh}}(k) \cdot v_{i,j}^{\text{veh}}(k)$$
(33)

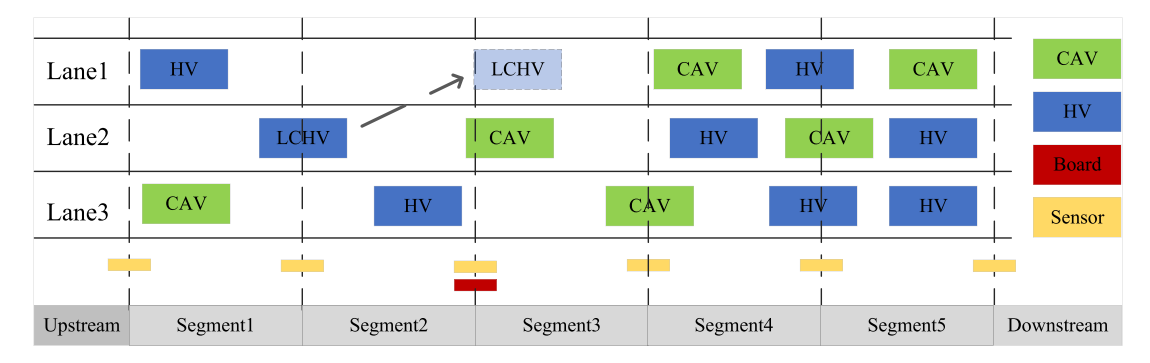


Fig. 5. Geometry of experiment road.

Table 3
Value of parameters.

Parameters Value		Parameters	Value	
Vehicle Simulat	or			
s_0	3 m	$b_{ m safe}$	2 m/s ²	
$b_{ m max}$	5 m/s ²	$b_{ m sharp}$	8 m/s^2	
τ	5 s	T	2 s	
γ	0.6	Δa	5 m/s^2	
a_{max}	5 m/s^2	u_f	120 km/h	
METANET and	LCTFM			
τ	20 s	ν	0.05	
κ	13 veh/km/lane	u_f	120 km/h	
$d_{\rm cr}$	33.5 veh/km	a	1.4324	
α	0.2			

5. Numerical study

In order to assess the performance of the lane-changing traffic flow model (LCTFM) proposed in this research, a series of numerical experiments are conducted. The primary focus of these experiments revolves around the estimation of traffic on a 3-lane highway, wherein varying VSL settings are employed within a mixed traffic environment. This section comprehensively elucidates the design of the numerical experiments concerning freeway geometry, mixed traffic flow simulation, model parameters, and measurements.

5.1. Freeway geometry

In the experiment, we have designed a 3-lane straight freeway with mixed traffic flow for model evaluation. The total length of this study area measures 5 km, divided into 5 segments, each spanning 1 km. Within this mixed traffic environment, we have a combination of CAVs and HVs. The HVs are capable of both car-following and lane-changing maneuvers.

As Fig. 5 shows, the sensors are installed along the roadside for data collection. Additionally, a speed control board is strategically positioned at the beginning of segment 3, indicating that segment 3 is the initial road segment where speed control measures are implemented.

5.2. Mixed traffic flow simulation

5.2.1. System logic

A mixed traffic simulator is designed for the numerical study in this research. The logic of the operation algorithm of this system is shown in Appendix D.

5.2.2. Parameters

The parameters employed in the experiment for both the vehicle trajectory simulator and the traffic model are documented in Table 3. The parameters utilized in the vehicle simulator serve to produce vehicle trajectories in a mixed traffic environment. The parameters for METANET(23) and LCTFM are configured to evaluate the performance of traffic model.

5.3. Measurements

To evaluate the performance of the proposed LCTFM, the error metrics Root Mean Squared Error (RMSE), Mean Absolute Percentage Error (MAPE), Mean Squared Prediction Error (MSPE) and Root Mean Squared Prediction Error (RMSPE) are applied.

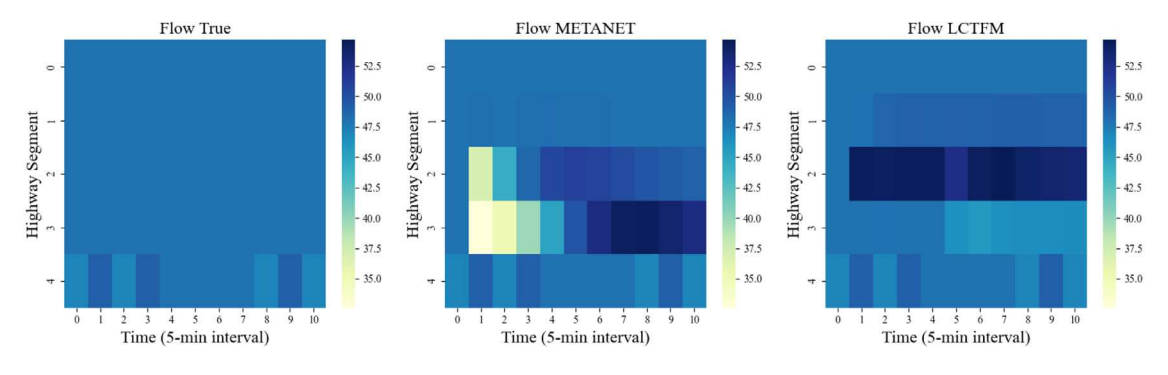


Fig. 6. Traffic flow estimation.

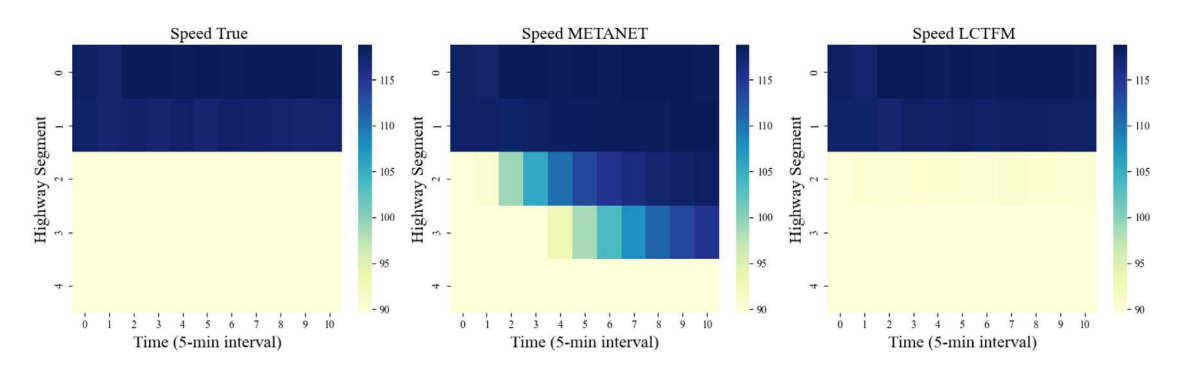


Fig. 7. Speed estimation.

The definitions of the error metrics are shown in the following equations.

$$RMSE = \sqrt{\frac{1}{N} \sum_{i=1}^{N} (x_i - \hat{x}_i)^2}$$
 (34)

$$MAPE = \frac{1}{N} \sum_{i=1}^{N} \left| \frac{x_i - \hat{x}_i}{\hat{x}_i} \right|$$
 (35)

$$MSPE = \frac{1}{N} \sum_{i=1}^{N} \left(\frac{x_i - \hat{x_i}}{\hat{x_i}} \right)^2$$
 (36)

$$RMSPE = \sqrt{\frac{1}{N} \sum_{i=1}^{N} \left(\frac{x_i - \hat{x}_i}{\hat{x}_i}\right)^2}$$
 (37)

where \hat{x}_i represents the value of estimation of mixed traffic flow model at each time step i; and x_i denotes the traffic flow data generated by the simulator.

6. Result analysis

6.1. Effectiveness analysis

The traffic status data is obtained from the vehicle trajectory data generated by the mixed traffic flow simulator. To evaluate the effectiveness of the multi-class traffic model presented in this study, we utilize the original METANET model as the reference for traffic status prediction.

Fig. 6 illustrates the model's performance in traffic flow estimation. It is evident that the predictive outcomes of the multi-class model closely match the actual traffic flow, outperforming the original METANET model. Notably, substantial improvements in the multi-class model's performance are observed, particularly after vehicle speed control, in segments 2, 3, and 4.

The proposed model shows a considerable improvement in traffic speed estimation. This enhancement is visually evident from Fig. 7, where it becomes apparent that the LCTFM outperforms the original METANET in accurately depicting the VSL. Notably, after passing the control spot, the majority of vehicles adhere to the speed limitation. In contrast to the original METANET's speed

Table 4Errors of model prediction.

	Traffic flow	Traffic flow		Traffic speed		
	METANET	LCTFM	METANET	LCTFM		
RMSE	3.830534	2.626936	16.7441	4.466233		
MAPE	0.037628	0.02925	0.115122	0.024635		
MSPE	0.006373	0.002997	0.029819	0.002122		
RMSPE	0.079803	0.054728	0.209676	0.055906		

estimation, which indicates an increase over time in speed along road sections after speed control, the proposed multi-class traffic model demonstrates a decrease in speed due to the influence of VSL.

In this case, the LCTFM achieved a substantially lower root mean square error (RMSE) of 2.626936 in traffic flow estimation, while the METANET model obtained a higher RMSE of 3.830534. Similarly, in traffic speed estimation, LCTFM obtained an RMSE of 4.466233, whereas the METANET model had a significantly higher RMSE of 16.7441. The lower RMSE values indicate that the LCTFM model outperforms the METANET model in accurately predicting traffic-related values.

MAPE computes the average percentage difference between predicted values and actual values. The results show that the LCTFM model outperforms the METANET model in both traffic flow and traffic speed prediction. The MAPE for LCTFM is 0.02925 in the traffic flow estimation and 0.024635 in the traffic speed prediction. In contrast, the METANET model yields higher MAPE values of 0.037628 and 0.115122 in the traffic flow and speed prediction, respectively. The lower MAPE values for LCTFM indicate that it provides more accurate predictions with smaller percentage errors. MSPE measures the average squared percentage differences between predicted and actual values. Once again, the LCTFM demonstrates superior performance, as it achieves lower MSPE values in both scenarios. The LCTFM's MSPE values are 0.002997 and 0.002122 in flow and speed estimation, respectively. On the other hand, the METANET model has higher MSPE values of 0.006373 and 0.029819 in the flow and speed estimation, respectively. The lower MSPE values for LCTFM highlight its ability to provide more precise predictions with minimized squared percentage errors. RMSPE computes the square root of the average squared percentage differences between predicted and actual values. As with the other metrics, the LCTFM performs better in this evaluation as well. It achieves RMSPE values of 0.054728 and 0.055906, while the METANET model has higher RMSPE values of 0.079803 and 0.209676 in flow and speed prediction respectively. The lower RMSPE values for LCTFM indicate its superior accuracy in predicting traffic-related values with minimized percentage errors (see Table 4).

In conclusion, the proposed model, by capturing the lane-changing behavior of HVs, offers a more comprehensive representation of the traffic status compared to the original METANET model, encompassing both speed and flow. The analysis of the performance metrics demonstrates that the LCTFM outperforms the METANET model in both traffic flow estimation and traffic speed prediction. It consistently exhibits lower values across all evaluation metrics, highlighting its superiority in accurately estimating traffic status.

6.2. Sensitive analysis on VSL difference

To further investigate the model's performance under various differences in VSL speeds, the experiments encompass diverse traffic flow scenarios. Specifically, the initial traffic speed is set at 120 km/h, while the speed limit assumes different lower values (110 km/h, 100 km/h, 90 km/h, 80 km/h, and 70 km/h). The analysis primarily centers on evaluating the extent of performance enhancement using RMSE, MAPE, MSPE, and RMSPE.

With different VSL speed, Fig. 8 illustrates the model's performance in estimating traffic flow, while Fig. 9 displays the predictions of traffic speed. Concerning traffic flow estimation, it is evident that as the disparity between the VSL and free flow speed increases, the flow variance at speed control section 2 becomes more pronounced. This is attributed to the greater influence of the speed limit on the traffic flow with a larger difference in VSL. Regarding traffic speed estimation, as the speed difference expands, the variance of the predicted speed also increases, indicating the model's effectiveness in predicting speed across different VSL values.

Table 5 reveals that the model's performance for both traffic flow and traffic speed estimation deteriorates (increased RMSE, MAPE, MSPE, and RMSPE) with a reduction in the speed limit from 120 km/h to 70 km/h. In contrast, the improvement demonstrated by LCTFM over the benchmark shows a progressive trend. This can be attributed to the fact that as the speed difference of VSL increases, there is a subsequent rise in the number of lane-changing events caused by the speed decrease of the leading vehicles. Consequently, the LCTFM proposed in this research, which takes into account the behavior of lane-changing vehicles, allows for a more accurate representation of the traffic flow status.

Regarding the traffic flow estimation, the LCTFM exhibits superior performance compared to the original METANET. The extent of improvement increases as the speed difference grows larger, leading to improvements of 34.61% in RMSE, 33.87% in MAPE, 57.24% in MSPE, and 34.61% in RMSE, respectively.

Concerning the speed estimation, the LCTFM also demonstrates significant enhancements over the benchmark. Notably, it exhibits greater improvements compared to the traffic flow estimation. This outcome can be attributed to the model proposed based on kinematic analysis of various vehicle categories, enabling the LCTFM proposed in this research to more accurately describe vehicle speeds and achieve superior overall performance.

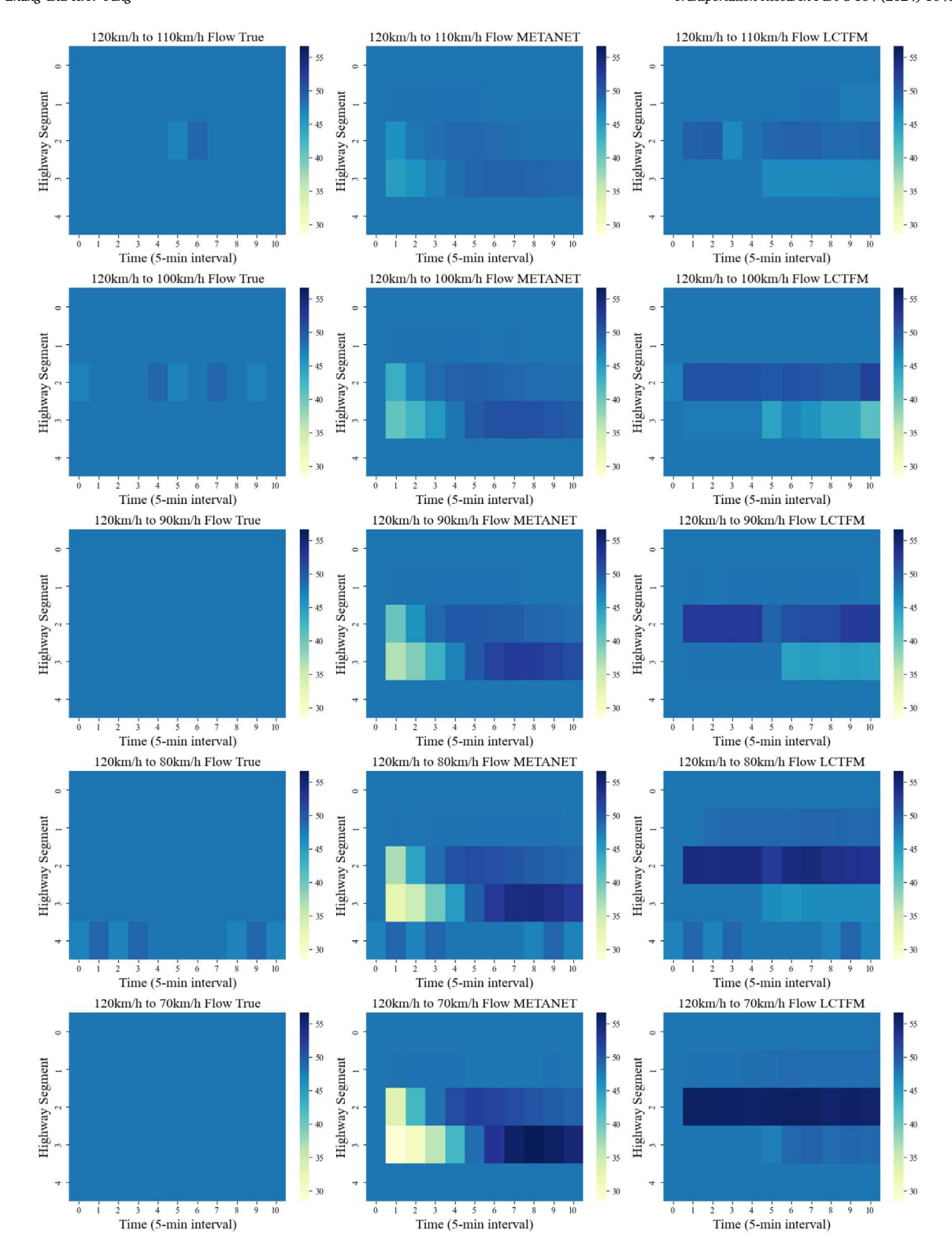


Fig. 8. Traffic flow estimation with different VSL speed.

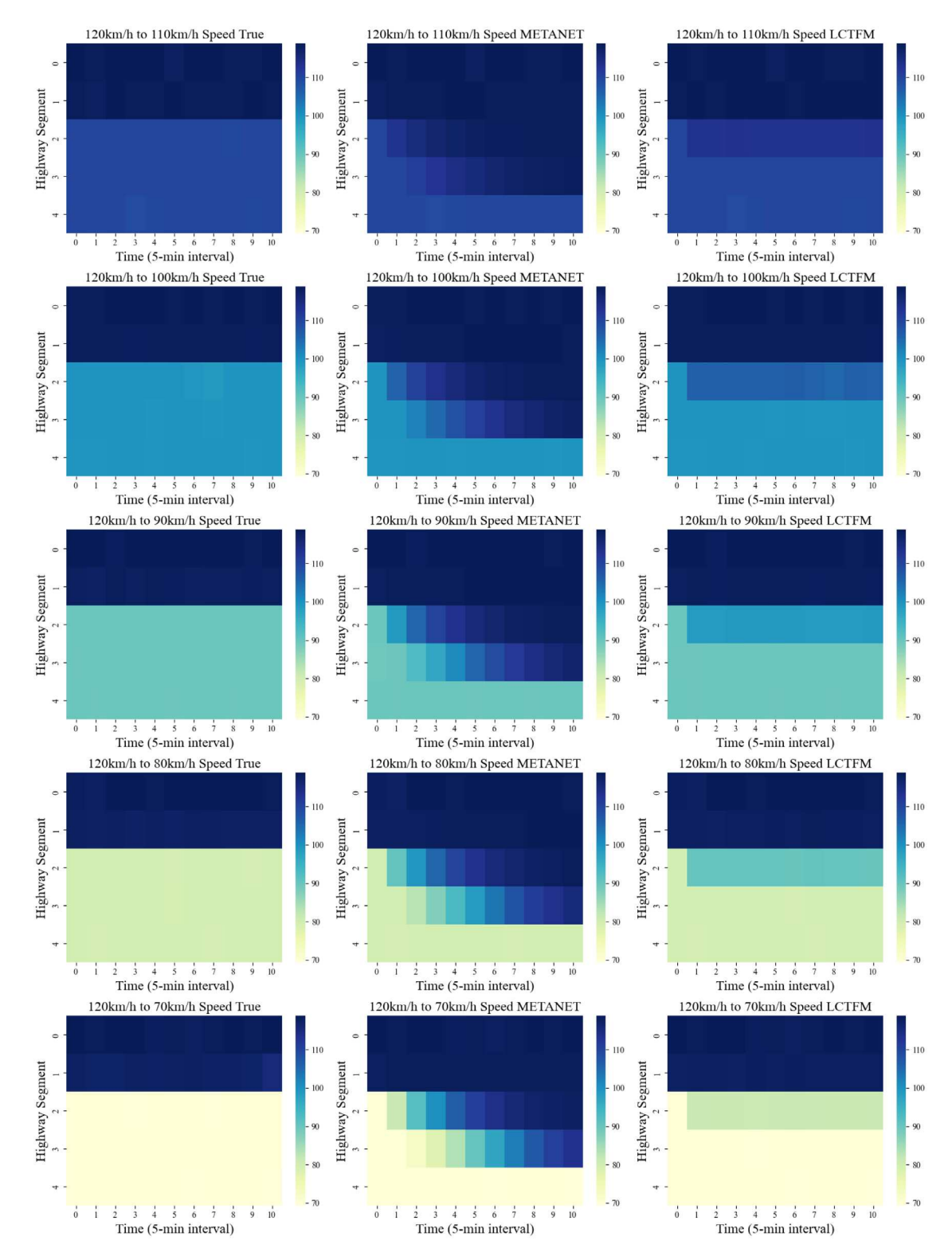


Fig. 9. Traffic speed estimation with different VSL speed.

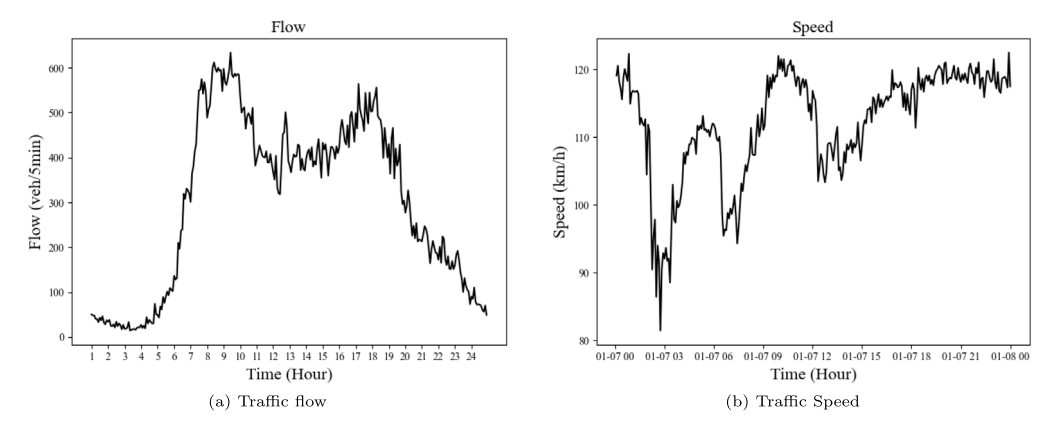


Fig. 10. Dynamic traffic flow data S406 on I-15.

Table 5
Errors of model prediction with different VSL speed.

	Traffic flow		Traffic speed			
	METANET	LCTFM	Improvement	METANET	LCTFM	Improvemen
120 km/h	to 110 km/h					
RMSE	0.755647	0.701197	7.21%	4.069715	1.435452	64.73%
MAPE	0.007795	0.007824	-0.37%	0.020998	0.00587	72.04%
MSPE	0.000248	0.000213	13.89%	0.001289	0.00016	87.56%
RMSPE	0.015773	0.014653	7.10%	0.03708	0.013076	64.74%
120 km/h	to 100 km/h					
RMSE	1.697376	1.694786	0.15%	8.681826	2.771797	68.07%
MAPE	0.016763	0.017818	-6.29%	0.048785	0.01234	74.71%
MSPE	0.001251	0.001248	0.30%	0.006516	0.000664	89.81%
RMSPE	0.035404	0.035372	0.09%	0.087197	0.027841	68.07%
120 km/h	to 90 km/h					
RMSE	2.691084	1.942346	27.82%	12.77466	3.734368	70.77%
MAPE	0.026262	0.021094	19.68%	0.07883	0.01832	76.76%
MSPE	0.003143	0.001637	47.90%	0.01561	0.001334	91.45%
RMSPE	0.056064	0.040466	27.82%	0.141936	0.041478	70.78%
120 km/h	to 80 km/h					
RMSE	3.830534	2.626936	31.42%	16.7441	4.466233	73.33%
MAPE	0.037628	0.02925	22.26%	0.115122	0.024635	78.60%
MSPE	0.006373	0.002997	52.97%	0.029819	0.002122	92.89%
RMSPE	0.079803	0.054728	31.42%	0.209676	0.055906	73.34%
120 km/h	to 70 km/h					
RMSE	5.111124	3.342379	34.61%	20.38392	4.947461	75.73%
MAPE	0.050117	0.033142	33.87%	0.158486	0.031353	80.22%
MSPE	0.011338	0.004849	57.24%	0.049022	0.002888	94.11%
RMSPE	0.106482	0.069633	34.61%	0.291951	0.070755	75.76%

6.3. Dynamic traffic flow analysis

To evaluate model performance in practice, experiments are conducted with dynamic traffic flow in this section. The simulation of mixed traffic flow trajectories is carried out using SUMO 1.19.0. In this experiment, traffic flow and speed undergo dynamic changes every 5 min. Real-world highway traffic data obtained from PeMS is utilized as traffic volume and speed in the mixed-traffic simulation, specifically, one-day traffic statistics data from Site S406 on I-15 on January 7, 2019, are employed. Fig. 10 illustrates the traffic patterns of flow and speed. The simulated 3-lane highway spans 5 km in length, with a VSL board situated at the 2 km mark, showing a speed limit of 90 km/h.

Figs. 11 and 12 depict the results of dynamic traffic estimation for flow and speed, respectively. During non-peak hours, both LCTFM and METANET demonstrate comparable performance in traffic flow estimation. Although occasional negative values are observed in the improvement column during these periods, the magnitude of differences among measurements is minimal. For instance, in the 18:00–24:00 time interval, the RMSE for traffic flow is 27.92 for METANET and marginally higher at 27.94 for LCTFM, indicating negligible variance between the two models during non-peak hours. However, during peak hours,

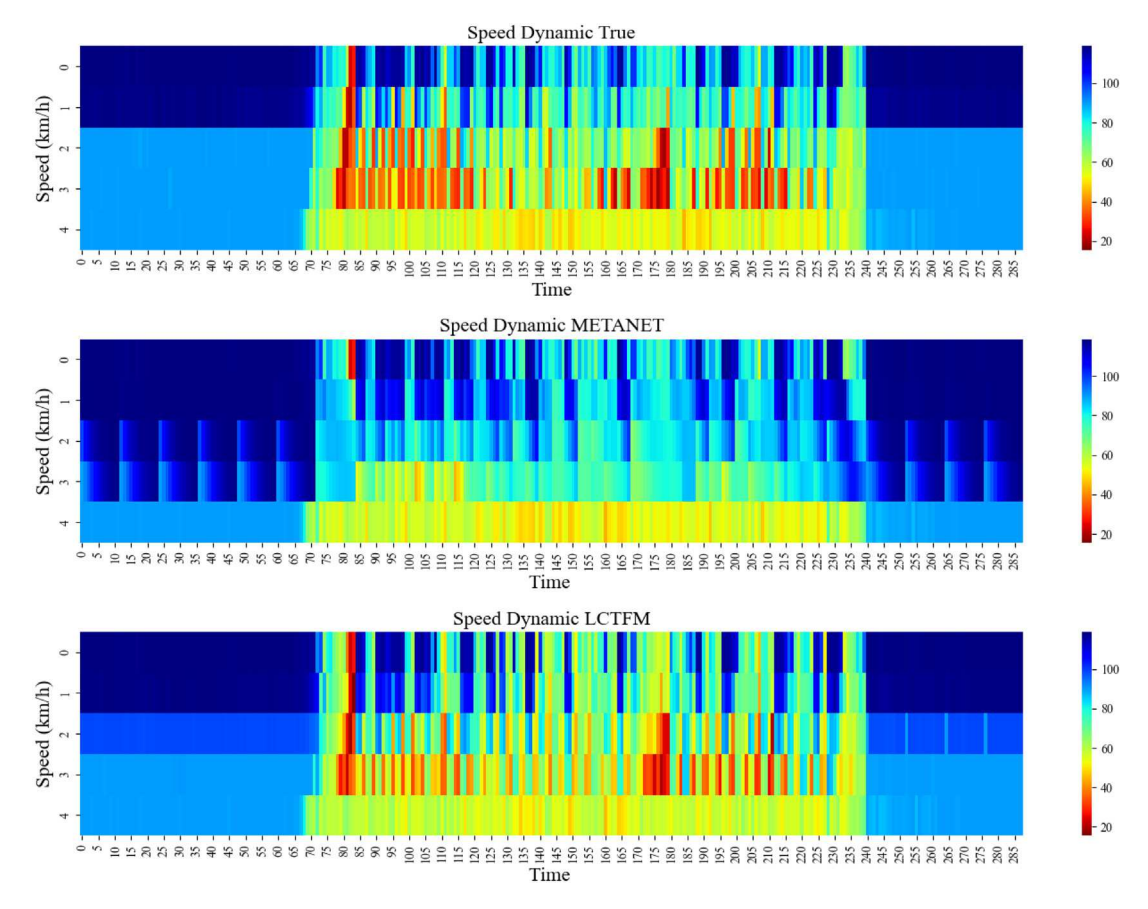


Fig. 11. Dynamic traffic speed estimation.

specifically from 6:00–9:00 and 15:00–18:00, LCTFM demonstrates a significant performance advantage over METANET in traffic flow estimation. In the morning peak hours (6:00–9:00), METANET exhibits an RMSE for traffic flow of 47.73, while LCTFM achieves a notably lower RMSE of 34.11. Similarly, during the evening peak hours (15:00–18:00), METANET shows an RMSE for traffic flow of 45.32, whereas LCTFM achieves a lower RMSE of 33.66, clearly illustrating the superior performance of LCTFM during periods of heightened traffic activity.

When it comes to speed estimation, LCTFM consistently outperforms METANET across all time intervals. For example, during the 0:00–6:00 period, METANET yields an RMSE of 14.34 for speed prediction, while LCTFM achieves a significantly lower RMSE of 4.46. Similarly, throughout peak hours, LCTFM maintains its superior performance in speed estimation, underscoring its efficacy in capturing the intricacies of traffic dynamics.

In conclusion, LCTFM presents itself as a promising model for improving the accuracy of traffic prediction in dynamic environments. During non-peak hours, the performance of METANET and LCTFM appears similar, owing to the lower traffic volume allowing drivers for more freely driving with ample space, resulting in fewer lane changes. However, during peak hours, when traffic volume increases, LCTFM outperforms METANET. This difference arises because as the number of vehicles increases, car-following distances decrease, leading to more frequent lane changes by human drivers. LCTFM focuses on the effects of lane-changing, which accounts for its better performance under these conditions (see Table 6).

7. Conclusion

The CAV technology holds promising benefits for road traffic management. In the long run, HVs and CAVs are expected to coexist and share the road network. To effectively support traffic management in this mixed traffic environment, it is essential to establish a fundamental traffic model theory. However, the conventional macroscopic traffic model faces critical challenges that need to be addressed, including: (a) Incorporating the lane-changing and car-following behaviors of HVs into the macroscopic traffic flow model to accurately capture the interaction between CAVs and HVs. (b) Developing a model for variable speed limit control that effectively accommodates both CAVs and HVs in a mixed traffic environment. (c) Properly accounting for the impact of the penetration rate and compliant rate of CAVs on the dynamics of traffic flow in freeway scenarios. Addressing these critical issues is essential to devise comprehensive traffic management strategies and ensure the seamless integration of CAVs and HVs in mixed traffic environments.

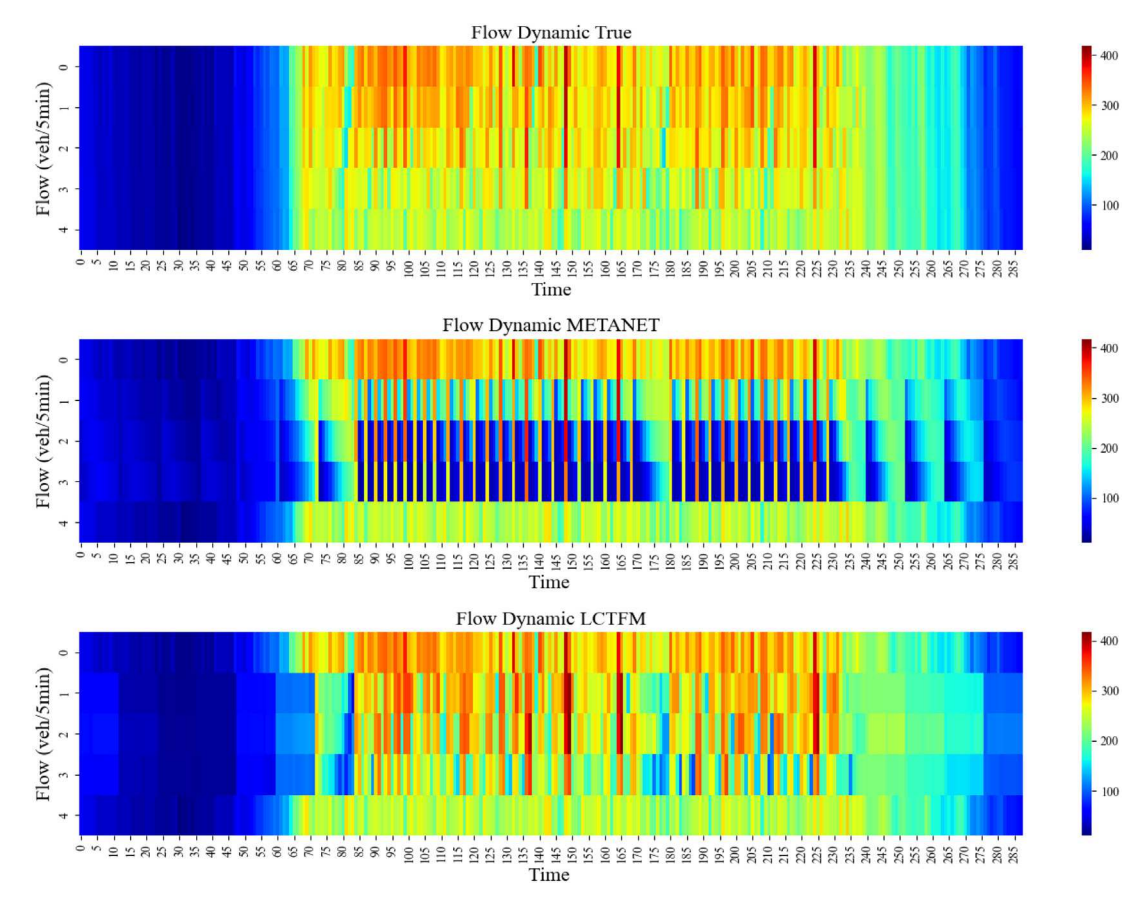


Fig. 12. Dynamic traffic flow estimation.

In this study, we introduce a discrete second-order macroscopic traffic model to bridge the existing gap. The proposed model categorizes vehicles into distinct classes, each possessing unique characteristics. Formulating the macroscopic model relies on the microscopic movement of each vehicle class, taking into account essential factors such as lane-changing and car-following behaviors. Additionally, the model effectively captures the intricate interaction between Connected and Autonomous Vehicles (CAVs) and Human-Operated Vehicles (HVs) arising from speed control. Moreover, both the penetration rate of CAVs and the compliant rate of HVs are incorporated into the framework of this model, contributing to its comprehensive and realistic representation of mixed traffic dynamics.

The numerical experiment was conducted to validate the performance of the proposed LCTFM. When compared to the original METANET model, the proposed model demonstrates a higher degree of accuracy in predicting the traffic status. Specifically, in terms of traffic flow estimation, the LCTFM exhibits significantly superior performance to the original METANET, with remarkable enhancements observed across the evaluation metrics. These improvements include a 34.61% reduction in RMSE, a 33.87% decrease in MAPE, a 57.24% decrease in MSPE, and a 34.61% decrease in RMSE, respectively. Regarding speed estimation, the LCTFM also showcases substantial advancements over the benchmark, surpassing the improvements observed in traffic flow estimation. This outcome can be attributed to the LCTFM being designed based on kinematic analysis of various vehicle categories, enabling it to more accurately capture vehicle speeds and achieve an overall superior performance compared to the original METANET model. On the other hand, the dynamic flow experiment compares the performance of METANET and LCTFM during both non-peak and peak traffic hours. During non-peak hours, both systems perform similarly due to lower traffic volume allowing for more relaxed driving conditions with fewer lane changes. However, during peak hours, LCTFM outperforms METANET. This is attributed to increased traffic volume, which reduces car-following distances and leads to more frequent lane changes by human drivers. LCTFM's focus on lane-changing behavior accounts for its superior performance under these conditions.

The proposed model holds the potential to facilitate various traffic control tasks in freeway management. By effectively estimating the mixed traffic status through current speed control on both CAVs and HVs, the model can contribute to more efficient traffic management strategies. Since the proposed model has been exclusively tested with a base case of 20% CAV penetration rate, exploring the effects of different penetration rates of CAVs could be a valuable subject for future research. Investigating pertinent issues related to varying rates of CAVs would offer valuable insights and enhance our understanding of the model's performance under different scenarios, thereby contributing to further advancements in traffic flow management in mixed-traffic environments.

Table 6 Errors of model prediction with dynamic traffic.

	Traffic flow			Traffic speed		
	METANET	LCTFM	Improvement	METANET	LCTFM	Improvement
0:00-6:00						
RMSE	19.484145	23.024619	-18.17%	14.343982	4.461923	68.89%
MAPE	19.230693	13.826918	28.10%	7.827990	2.028493	74.09%
MSPE	0.028607	0.014946	47.75%	0.003247	0.000255	92.16%
RMSPE	0.345821	0.259399	24.99%	0.169094	0.055247	67.33%
Morning Pe	eak: 6:00–9:00					
RMSE	47.731768	34.112328	28.53%	28.710381	16.757571	41.63%
MAPE	10.998845	10.312187	6.24%	48.894659	21.672432	55.68%
MSPE	0.000055	0.000049	10.01%	0.016610	0.003657	77.98%
RMSPE	0.179710	0.188256	-4.76%	0.846426	0.424577	49.84%
9:00-15:00	1					
RMSE	46.862666	43.777104	6.58%	26.664435	10.077302	62.21%
MAPE	11.326111	9.440654	16.65%	47.760446	12.468550	73.89%
MSPE	0.000066	0.000040	38.99%	0.017008	0.001585	90.68%
RMSPE	0.200232	0.168005	16.09%	0.697024	0.233139	66.55%
Evening Pe	eak: 15:00–18:00					
RMSE	45.321898	33.662123	25.73%	25.532131	11.297092	55.75%
MAPE	9.188097	7.720175	15.98%	47.940067	14.809010	69.11%
MSPE	0.000040	0.000030	25.53%	0.015921	0.002434	84.71%
RMSPE	0.171894	0.143504	16.52%	0.724282	0.275972	61.90%
18:00-24:0	0					
RMSE	27.923541	27.937251	-0.05%	17.215965	5.669504	67.07%
MAPE	10.341115	10.780485	-4.25%	16.263195	4.382192	73.05%
MSPE	0.000213	0.000346	-62.71%	0.001622	0.000227	85.99%
RMSPE	0.170328	0.180110	-5.74%	0.254897	0.084139	66.99%

CRediT authorship contribution statement

Yi Zhang: Writing - original draft, Methodology, Investigation, Data curation. Xianfeng (Terry) Yang: Writing - review & editing, Validation, Supervision, Funding acquisition, Conceptualization.

Acknowledgments

This study is supported by the grant titled "CAREER: Physics Regularized Machine Learning Theory: Modeling Stochastic Traffic Flow Patterns for Smart Mobility Systems", funded by the National Science Foundation. The authors would like to acknowledge the utilization of ChatGPT, a large language model, exclusively for enhancing the linguistic quality of the manuscript preparation process.

Appendix A. Proportion analysis of lane-changing HVs

The proportion of LCHV is related to the traffic flow status and lane-changing conditions. Human drivers are assumed to be greedy, as long as the lane-changing conditions are satisfied, the driver will change lanes to ensure that the driving speed will not be affected by the deceleration of the leading vehicle. Drivers are also assumed to change their lanes only once per time interval.

For two homogeneous adjacent lanes j and j + 1 in segment i, if the vehicle on lane j intend to switch to lane j + 1, the vehicle space on lane j + 1 $s_{j+1}^{initial}$ should satisfy both safe distance (Eq. (3)) and advantage distance (Eq. (4)).

$$s_{j+1}^{initial} \ge S_{safe} + S_{adv} \tag{38}$$

$$S_{j,j+1}^{initial} = S_{safe} + S_{adv} = s_0 + T \left[v_{j+1}^{initial} + \tau (\Delta a + a_{bias} - b_{safe}) \right] + s_j^{initial}$$

$$(39)$$

Assume $n_{j,j+1}$ human-drivers will change their lane from j to j+1, the final number of HVs on lane j+1 after lane-changing will be $n_{j+1}^{initial} + n_{j,j+1}$, and the number of HVs on lane j will be $n_{j+1}^{initial} - n_{j,j+1}$. The traffic density after lane-changing for lane j and j+1 could be $\frac{n_{j+1}^{initial} - n_{j,j+1}}{L}$ and $\frac{n_{j+1}^{initial} + n_{j,j+1}}{L}$ respectively; and car-following distance after lane-changing for lane j and j+1 is $\frac{L}{n_{j+1}^{initial} - n_{j,j+1}}$ and $\frac{1}{n_{j+1}^{lmit}ll} \frac{l}{n_{j,j+1}}$.

After the lane-changing, the vehicle distance on lane j+1 will be less than:

$$s_{i+1}^{final} \ge S_{i,i+1}^{final} \tag{40}$$

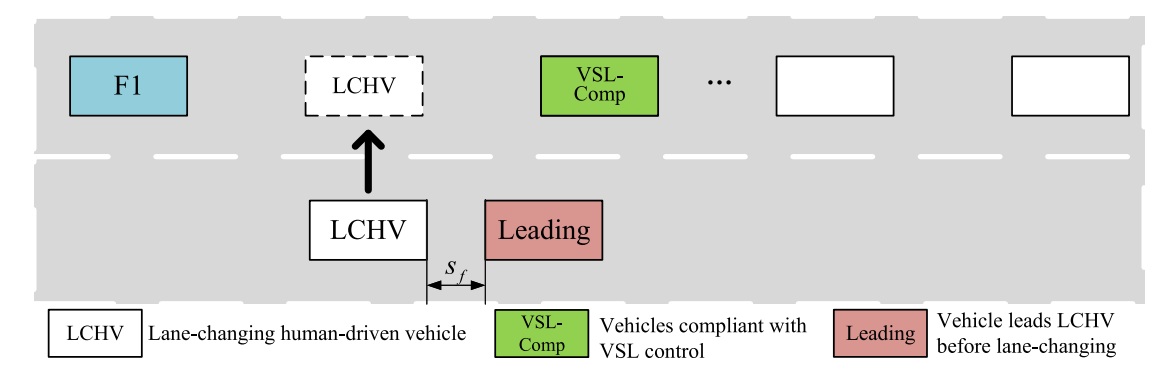


Fig. 13. LCHV follows a VSL-compliant vehicle after lane-changing.

$$S_{i,i+1}^{final} = s_0 + T \left[v_{i+1}^{final} + \tau (\Delta a + a_{bias} - b_{safe}) \right] + s_j^{final}$$
(41)

Because the drivers are greedy, they will try to change lanes if the lane-changing conditions are satisfied. As vehicles change lanes from lane j to j + 1, the traffic density in lane j + 1 increases, while the car-following distance decreases. Lane j + 1 could accommodate vehicles from lane j until the car-following distance of lane j + 1 does not meet the lane-changing conditions.

Considering the relation between the number of lane-changing vehicles from lane j to j + 1 and the car-following distance on lane j + 1, the equilibrium of lane-changing of adjacent lanes j and j + 1 in segment i could be described as:

$$\frac{L}{n_{j+1}^{initial} + n_{j,j+1}} = s_0 + \frac{L}{n_j^{initial} - n_{j,j+1}} + T\tau(\Delta a + a_{bias} - b_{safe})
+ Tv_{f,i,j+1} \exp\left[\frac{1}{a_{i,j+1}} \left(\frac{n_{j+1}^{initial} + n_{j,j+1}}{Ld_{cr,i,j+1}}\right)^{a_{i,j+1}}\right]$$
(42)

In the Eq. (42), the number of lane-changing vehicles $n_{i,i,j+1}$ from lane j to lane j+1 on segment i could be calculated.

Appendix B. Proof of the Lemmas

Lemma 1. In a given road segment, a higher proportion of VSL-compliant vehicles leads to a shorter platoon length. platoon length. Assume there are n vehicles in road segment i lane j. The proportion p of VSL-compliant vehicles could be calculated as:

$$p_{i,i} = \alpha_{i,i} + \beta_{i,i} \tag{43}$$

Then, the length of the platoon is $\frac{1}{\alpha_{i,j}+\beta_{i,j}}$. As the parameter $p_{i,j}$ increases, the reciprocal of $(\alpha_{i,j}+\beta_{i,j})$ decreases, resulting in a reduction in the platoon's length. In summary, in a given road segment, a higher proportion of VSL-compliant vehicles leads to a shorter platoon length. Proved.

Lemma 2. The further a CAV or a CHV is from the LCHV, the later the LCHV will decelerate its speed.

In the absence of a lane change, the HV should reduce its speed when the preceding vehicle in the current lane slows down. Due to the advantageous condition, the HV can maintain a higher speed in the adjacent lane after the lane change than in its original lane. Assume the LCHV gets into the target lane at t_0 , the car-following distance of LCHV is:

$$s_{LCHV}(t) = s_e + \int_{t_0}^t v_{\hat{I}}(t) dt - \int_{t_0}^t v_{LCHV}(t) dt$$
(44)

Car-following behavior is contingent on the car-following distance; when the car-following distance exceeds the threshold distance s_{cf} , alterations in the leading vehicle's velocity do not affect the trailing vehicle.

Case 1: If the LCHV follows a VSL-compliant vehicle after lane-changing (Fig. 13) with $s_{\rm LCHV} > s_{cf}$ and the VSL-compliant vehicle passes a VSL control spot at t_{vsl} with $v^{VSL} < v_{\hat{l}}(t_{vsl})$, the LCHV will start to decrease speed when the car-following distance $s_{\rm LCHV} = s_{cf}$ at t_{dec} :

$$s_{cf} = s_e + \int_{t_{vsl}}^{t_{dec}} v_{\hat{l}}(t) dt - \int_{t_{vsl}}^{t_{dec}} v_{\text{LCHV}}(t) dt$$
 (45)

$$s_{cf} - s_e = \int_{t_{vsl}}^{t_{dec}} v_{\hat{l}}(t) - v_{\text{LCHV}}(t) dt$$
 (46)

$$\Delta t = t_{dec} - t_{vsl} \tag{47}$$

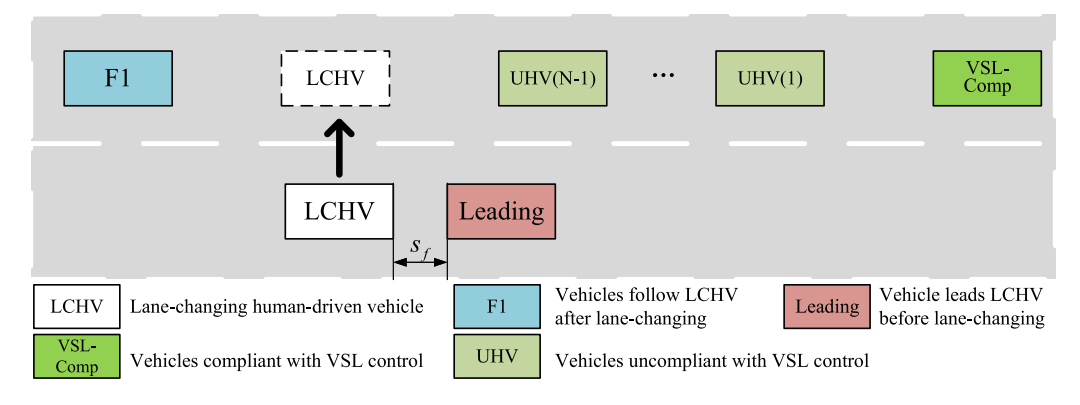


Fig. 14. LCHV follows an N-vehicle platoon after lane-changing.

Case 2: If the LCHV follows an N-vehicle platoon after lane-changing (Fig. 14), the platoon should be in equilibrium status without the VSL control, and the car-following distance for *i*th UHV in the platoon should be $s_{UHV_i} = s_e > s_{cf}$. Assume the VSL-compliant vehicle passes a VSL control spot at t_{vsl} with $v^{VSL} < v_{\hat{l}}(t_{vsl})$, the first UHV will start to decrease speed when the car-following distance $s_{UHV_i} = s_{cf}$ at t_{dec_1} :

$$s_{cf} - s_e = \int_{t_{rel}}^{t_{dec_1}} v_{\hat{l}}(t) - v_{UHV_1}(t) dt$$
(48)

$$\Delta t_1 = t_{dec_1} - t_{vsl} \tag{49}$$

When v^{VSL} in Case 1 is equal to the speed limit in Case 2, $\Delta t = \Delta t_1$. Similarly, the *i*th UHV will start to decrease speed at t_{dec} :

$$s_{cf} - s_e = \int_{t_{dec_{i-1}}}^{t_{dec_i}} v_{UHV_{i-1}}(t) - v_{UHV_i}(t) dt$$
(50)

The LCHV will start to decrease its speed when its car-following distance at t_{dec} ,

$$t_{dec} = t_{vsl} + \sum_{i=1}^{N} \Delta t_i = t_{vsl} + \Delta t_1 + \sum_{i=2}^{N} \Delta t_i = t_{vsl} + \Delta t + \sum_{i=2}^{N} \Delta t_i$$
 (51)

 $\sum_{i=2}^{N} \Delta t_i > 0$... t_{dec} in Case 2 is larger than t_{dec} in Case 1. In other words, the further a CAV or a CHV is from the LCHV, the later the LCHV will decelerate its speed.

Proved.

Appendix C. Proof of the Theorem

Assume the LCHV follows a 3-vehicle platoon after lane-changing, the first vehicle is a VSL-compliant vehicle, which is also the leading vehicle of this platoon, and the second and third vehicles are UHVs (see Fig. 15).

In this platoon, the moving of the leading vehicle could be described as:

$$\dot{v}_{lead}(t) = \frac{V^{VSL}(s(t)) - v_{lead}(t)}{\tau} \tag{52}$$

For the UHVs in the platoon following the VSL-compliant vehicle, the car-following model could be written as:

$$\dot{v}_m(t) = \frac{V^{free}(s(t)) - v_m(t)}{\tau} - \gamma(v_m(t) - v_{m+1}(t)) \tag{53}$$

Then, the car-following model of this LCHV could be written as:

$$\dot{v}_{LCHV}(t,3) = \frac{V(s_1(t) - v_{LCHV}(t))}{\tau} - \frac{v_{LCHV}(t)}{L} \left(v_{LCHV}(t) - v_{UHV1}(t) \right) \tag{54}$$

From the Eq. (6), the velocity function of vehicles in the platoon could be written as:

$$v_{UHV1}(t + \Delta t) = v_{UHV1}(t) + \Delta t \left(\frac{V(s_2(t) - v_{UHV1}(t))}{\tau} - \frac{v_{UHV1}(t)}{L} \left(v_{UHV1}(t) - v_{UHV2}(t) \right) \right)$$
 (55)

$$v_{UHV2}(t + \Delta t) = v_{UHV2}(t) + \Delta t \left(\frac{V(s_3(t) - v_{UHV2}(t))}{\tau} - \frac{v_{UHV2}(t)}{L} \left(v_{UHV2}(t) - v_{lead}(t) \right) \right)$$
 (56)

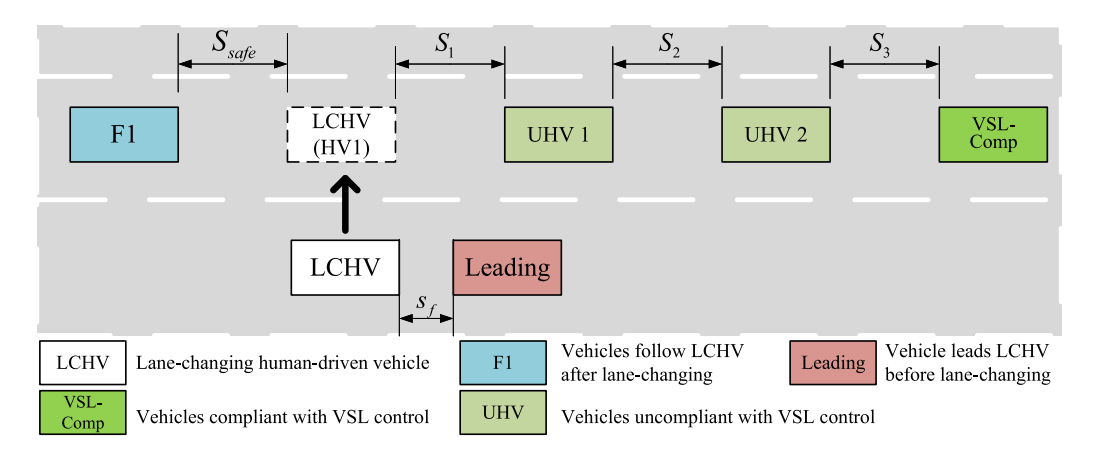


Fig. 15. The situation of 3 vehicles before the LCHV.

$$v_{lead}(t + \Delta t) = v_{lead}(t) + \frac{v^{VSL} - v_{lead}(t)}{\tau}$$
(57)

 $\because v(t) = \lim_{\Delta t \to 0} v(t + \Delta t)$

∴ In Eq. (57), $v_{lead}(t) = \lim_{\Delta t \to 0} v_{lead}(t + \Delta t)$; $v_{UHV2}(t) = \lim_{\Delta t \to 0} v_{UHV2}(t + \Delta t)$ in Eq. (56); $v_{UHV1}(t) = \lim_{\Delta t \to 0} v_{UHV1}(t + \Delta t)$ in Eq. (55).

After the replacement and reorganization, the acceleration function of LCHV following a 3-vehicle platoon could be written as

$$\dot{v}_{LCHV}(t,3) = \sum_{n=1}^{3} \left[\frac{\Delta t}{L}^{n-1} \left(\frac{V(s_n(t)) - v_n(t)}{\tau} - \frac{v_n(t)(v_n(t) - v_{n+1}(t))}{L} \right) \prod_{n=1}^{2} v_n(t) \right]$$
(58)

To get the general formulation, replace 3 with N in Eq. (58). If there are N vehicles before an LCHV. The leading vehicle is a VSL-compliant vehicle, and the N-1 followed vehicles are UHV. The acceleration function of time could be written as:

$$\dot{v}_{LCHV}(t,N) = \sum_{n=1}^{N} \left[\frac{\Delta t}{L}^{n-1} \left(\frac{V(s_n(t)) - v_n(t)}{\tau} - \frac{v_n(t)(v_n(t) - v_{n+1}(t))}{L} \right) \prod_{n=1}^{N-1} v_n(t) \right]$$
(59)

Proved.

Appendix D. The operation logic of the simulator

In this study, the simulator is developed to model car-following and lane-changing behaviors in multi-lane mixed traffic scenarios. The overall structure of the simulator is illustrated in **Algorithm 1**, which consists of the vehicle initialization module **Algorithm 2**, CAV operation module **Algorithm 3**, LCHV operation module **Algorithm 4**, and HV operation module **Algorithm 5**.

The vehicle initialization module is designed to generate vehicles dynamically as the traffic status may change in different calculating periods (for example, 5 min) during the whole simulation process. Then, the simulated traffic flow will be more similar to the real-world traffic flow with time-varying traffic status.

The CAV operation module describes the moving of CAVs in the mixed-traffic environment. CAVs will follow the previous vehicle and be controlled by the activated VSL speed.

The LCHV operation module describes the lane-changing behavior. In practice, the lane-changing process typically spans a time interval of 1–1.5 s rather than occurring instantaneously. Consequently, the lane-changing count is employed to characterize this temporal aspect of the process. In addition, the lane-changing vehicle's movement is influenced by preceding vehicles in both its current and target lanes, necessitating the adoption of the minimum acceleration value from both lanes.

In the HV operation module, the lane-changing judgment describes the decision-making process for lane changes. If the lane-changing conditions and random factor condition are satisfied, the current HV will commence the lane-changing process in the subsequent time step; otherwise, it will update its status through car-following.

Fig. 16 illustrates the time-space pattern of vehicles in each lane, depicting their trajectories and corresponding speeds with the trajectory color. The initial flow and speed for the simulation are based on the peak hour volume of the S406 on I-15 in the PeMS dataset. The speed was controlled to decrease to 90 km/h after passing the designated control spot at 2000 m. When the traffic flow is lower, the figure demonstrates a noticeable decrease in the gradient of vehicle trajectories, signifying a decrease in vehicle

Algorithm 1: Mixed traffic multi-lane simulator

```
1 Start
2 if Accumulate simulation time < Total simulation time then
      if mod(Accumulate simulation time / Flow update interval)=0 then
          Run vehicle initialization module
 4
      for Each vehicle in vehicle matrix do
5
          In-system Judgement:
 6
          if Vehicle in-system status is activated then
 7
             if The vehicle is a CAV then
                 Run CAV operation module
             if The vehicle is a LCHV then
10
                 Run LCHV operation module
11
             if The vehicle is a HV then
12
                 Run HV operation module
13
             In-system Adjustment
14
             if Vehicle position still in experiment area then
15
                 Vehicle in-system status activated
16
              else
17
              The vehicle finished the experiment, vehicle in-system status inactivated
18
19
          else
20
              Vehicle in-system status is inactivated;
              Goes to the next vehicle.
21
      Accumulate simulation time update
22
23
  else
      Simulation End
  Output: The trajectory sets include vehicle lane number, speed, acceleration, and position of all vehicles.
```

Algorithm 2: Vehicle initialization module

Input: Traffic flow, speed, vehicle proportion gathered in time interval; Speed variance, Car-following distance variance; Number of lanes

- 1 Step1 Calculate the vehicle number in the current update interval and generate the vehicle set for each lane.
- 2 Step2 Generate vehicle type randomly with vehicle proportion.
- 3 Step3 Generate vehicle speed and car-following distance based on the traffic speed, traffic density, and variance.
 - Output: Vehicle matrix with initial speed, position, vehicle type

Algorithm 3: CAV operation module

Input: CAV position, speed, acceleration; Front vehicle position, speed, acceleration; VSL speed and position

- 1 **Step1** Calculate the acceleration for the next step
- 2 if CAV is under VSL control then
- 3 Desired speed = VSL speed
- 4 if CAV is not under VSL control then
- 5 Desired speed = Free flow speed
- 6 Step2 Calculate the speed for the next step
- 7 Step3 Calculate the position for the next step
 - Output: CAV position, speed, acceleration for next simulation step

speed after passing the control point. Conversely, higher traffic flow leads to the generation of shockwaves. Furthermore, the figure reveals that lane 2 exhibited a higher initial traffic density compared to lanes 1 and 3. As a result, vehicles in lanes with higher initial density, such as lane 2, demonstrated a greater tendency to switch to lanes with lower density after receiving the speed decrease command.

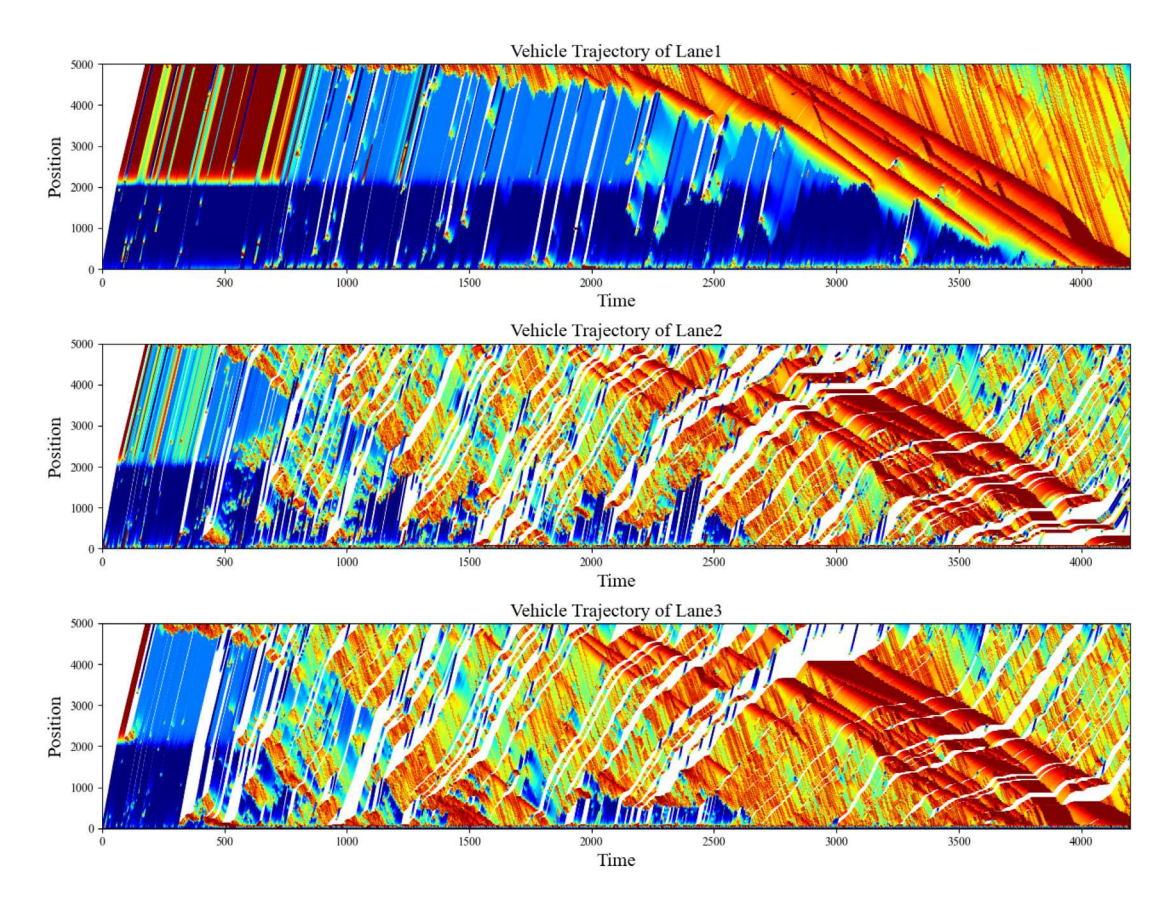


Fig. 16. Vehicle trajectory in 3 lanes simulation.

Algorithm 4: LCHV operation module

Input: LCHV position, speed, acceleration; Front vehicle position, speed, acceleration in both origin lane and target lane; Free flow speed; Lane-changing count

- 1 **Step1** Calculate the acceleration for the next step, $a_{next} = min\{a_{current}, a_{target}\}$
- 2 Step2 Calculate the speed for the next step
- 3 Step3 Calculate the position for the next step
- 4 Step4 Update lane-changing count
- $\ \ \text{if Lane-changing count} < \textit{Lane-changing time then} \\$
- 6 Vehicle still in the lane-changing process, vehicle type for the next step is LCHV
- 7 else
- Vehicle finished lane-changing, the vehicle type change to HV, vehicle lane number = target lane

 Output: LCHV position, speed, acceleration, lane number for next simulation step

Algorithm 5: HV operation module

Vehicle type is UHV;

Desired speed = Free flow speed

Step2-1 Calculate the acceleration for the next step

Step2-2 Calculate the speed for the next step **Step2-3** Calculate the position for the next step

Input: HV position, speed, acceleration; Front vehicle position, speed, acceleration in both origin lane and adjacent lane(s); Free flow speed; VSL speed and position 1 Check the lane-changing conditions 2 if Both conditions are satisfied, random selection satisfied then The vehicle will start lane-changing; 3 **Step1-1** Calculate the acceleration for the next step, $a_{next} = min\{a_{current}, a_{target}\}$ 4 Step1-2 Calculate the speed for the next step 5 Step1-3 Calculate the position for the next step 6 Step1-4 lane-changing count = 0; record the target lane number 7 8 else The vehicle will keep car-following; if Vehicle type is CHV then 10 if Vehicle is under VSL control then 11 Desired speed = VSL speed 12 if Vehicle is not under VSL control then 13 Desired speed = Free flow speed 14 else 15

Output: HV position, speed, acceleration, lane number, target lane number, lane-changing status, and lane-changing count for next simulation step

References

16

17

18 19

20

Ahmed, K.I., 1999. Modeling Drivers' Acceleration and Lane Changing Behavior (Ph.D. thesis). Massachusetts Institute of Technology.

An, L., Yang, X., Hu, J., 2022. Modeling system dynamics of mixed traffic with partial connected and automated vehicles. IEEE Trans. Intell. Transp. Syst. 23 (9), 15755–15764.

Asaithambi, G., Kanagaraj, V., Srinivasan, K.K., Sivanandan, R., 2018. Study of traffic flow characteristics using different vehicle-following models under mixed traffic conditions. Transp. Lett. 10 (2), 92–103.

Bando, M., Hasebe, K., Nakayama, A., Shibata, A., Sugiyama, Y., 1995. Dynamical model of traffic congestion and numerical simulation. Phys. Rev. E 51 (2),

Bose, A., Ioannou, P.A., 2003. Analysis of traffic flow with mixed manual and semiautomated vehicles. IEEE Trans. Intell. Transp. Syst. 4 (4), 173-188.

Chanut, S., Buisson, C., 2003. Macroscopic model and its numerical solution for two-flow mixed traffic with different speeds and lengths. Transp. Res. Rec. 1852 (1), 209–219.

Du, R., Chen, S., Li, Y., Dong, J., Ha, P.Y.J., Labi, S., 2020. A cooperative control framework for CAV lane change in a mixed traffic environment. arXiv preprint arXiv:2010.05439.

Guo, Q., Ban, X.J., 2020. Macroscopic fundamental diagram based perimeter control considering dynamic user equilibrium. Transp. Res. B 136, 87-109.

Guo, Q., Ban, X.J., Aziz, H.A., 2021. Mixed traffic flow of human driven vehicles and automated vehicles on dynamic transportation networks. Transp. Res. C 128, 103159.

Guo, X.Y., Zhang, G., Jia, A.F., 2023. Study on mixed traffic of autonomous vehicles and human-driven vehicles with different cyber interaction approaches. Veh. Commun. 39, 100550.

Halakoo, M., Yang, H., 2021. Evaluation of macroscopic fundamental diagram transition in the era of connected and autonomous vehicles. In: 2021 IEEE Intelligent Vehicles Symposium. IV, IEEE, pp. 1188–1193.

He, S., Ding, F., Lu, C., Qi, Y., 2022. Impact of connected and autonomous vehicle dedicated lane on the freeway traffic efficiency. Eur. Transp. Res. Rev. 14 (1), 12.

Hegyi, A., De Schutter, B., Hellendoorn, H., 2005. Model predictive control for optimal coordination of ramp metering and variable speed limits. Transp. Res. C 13 (3), 185–209.

Hu, X., Wang, W., Yang, H., 2012. Mixed traffic flow model considering illegal lane-changing behavior: Simulations in the framework of Kerner's three-phase theory. Physica A 391 (21), 5102–5111.

Huang, K., Yang, X., Lu, Y., Mi, C.C., Kondlapudi, P., 2018. Ecological driving system for connected/automated vehicles using a two-stage control hierarchy. IEEE Trans. Intell. Transp. Syst. 19 (7), 2373–2384.

Jiang, R., Wu, Q., Zhu, Z., 2001. Full velocity difference model for a car-following theory. Phys. Rev. E 64 (1), 017101.

Jin, W.L., 2010. Macroscopic characteristics of lane-changing traffic. Transp. Res. Rec. 2188 (1), 55-63.

Jin, I.G., Orosz, G., 2016. Optimal control of connected vehicle systems with communication delay and driver reaction time. IEEE Trans. Intell. Transp. Syst. 18 (8), 2056–2070.

Kavas-Torris, O., Gelbal, S.Y., Cantas, M.R., Guvenc, B.A., Guvenc, L., 2021. Connected UAV and CAV Coordination for Improved Road Network Safety and Mobility. Technical Report, SAE Technical Paper.

Koshy, R.Z., Arasan, V.T., 2005. Influence of bus stops on flow characteristics of mixed traffic. J. Transp. Eng. 131 (8), 640-643.

Kotsialos, A., Papageorgiou, M., Diakaki, C., Pavlis, Y., Middelham, F., 2002. Traffic flow modeling of large-scale motorway networks using the macroscopic modeling tool METANET. IEEE Trans. Intell. Transp. Syst. 3 (4), 282–292.

- Laval, J.A., Leclercq, L., 2008. Microscopic modeling of the relaxation phenomenon using a macroscopic lane-changing model. Transp. Res. B 42 (6), 511–522. Levin. M.W.. Boyles, S.D., 2016. A multiclass cell transmission model for shared human and autonomous vehicle roads. Transp. Res. C 62, 103–116.
- Li, X., Xiao, Y., Zhao, X., Ma, X., Wang, X., 2023. Modeling mixed traffic flows of human-driving vehicles and connected and autonomous vehicles considering human drivers' cognitive characteristics and driving behavior interaction. Physica A 609, 128368.
- Liu, S., De Schutter, B., Hellendoorn, H., 2014. Model predictive traffic control based on a new multi-class metanet model. IFAC Proc. Vol. 47 (3), 8781–8786. Liu, S., Hellendoorn, H., De Schutter, B., 2016. Model predictive control for freeway networks based on multi-class traffic flow and emission models. IEEE Trans. Intell. Transp. Syst. 18 (2), 306–320.
- Lo, S.C., Hsu, C.H., 2010. Cellular automata simulation for mixed manual and automated control traffic. Math. Comput. Model. 51 (7-8), 1000-1007.
- Lu, Q., Tettamanti, T., Hörcher, D., Varga, I., 2020. The impact of autonomous vehicles on urban traffic network capacity: an experimental analysis by microscopic traffic simulation. Transp. Lett. 12 (8), 540–549.
- Ma, L., Qu, S., Ren, J., Zhang, X., 2023. Mixed traffic flow of human-driven vehicles and connected autonomous vehicles: String stability and fundamental diagram. Math. Biosci. Eng. 20, 2280–2295.
- Meng, J.p., Dai, S.q., Dong, L.y., Zhang, J.f., 2007. Cellular automaton model for mixed traffic flow with motorcycles. Physica A 380, 470-480.
- Messmer, A., Papageorgiou, M., 1990. METANET: a macroscopic simulation program for motorway networks. Traffic Eng. Control 31, 466-470.
- Ngoduy, D., Hoogendoorn, S., Liu, R., 2009. Continuum modeling of cooperative traffic flow dynamics. Physica A 388 (13), 2705-2716.
- Papadoulis, A., Quddus, M., Imprialou, M., 2019. Evaluating the safety impact of connected and autonomous vehicles on motorways. Accid. Anal. Prev. 124, 12–22
- Peng, B., Keskin, M.F., Kulcsár, B., Wymeersch, H., 2021. Connected autonomous vehicles for improving mixed traffic efficiency in unsignalized intersections with deep reinforcement learning. Commun. Transp. Res. 1, 100017.
- Qin, Y., Wang, H., 2019. Cell transmission model for mixed traffic flow with connected and autonomous vehicles. J. Transp. Eng. A Syst. 145 (5), 04019014. Rahman, M., Chowdhury, M., Xie, Y., He, Y., 2013. Review of microscopic lane-changing models and future research opportunities. IEEE Trans. Intell. Transp. Syst. 14 (4), 1942–1956.
- Seraj, M., Li, J., Qiu, T.Z., 2020. Expansion of the fundamental diagram from a microscopic multilane modeling framework of mixed traffic. J. Adv. Transp. 2020, 1–15.
- Shi, X., Li, X., 2021. Constructing a fundamental diagram for traffic flow with automated vehicles: Methodology and demonstration. Transp. Res. B 150, 279–292.
- Tajdari, F., Roncoli, C., 2021. Adaptive traffic control at motorway bottlenecks with time-varying fundamental diagram. IFAC-PapersOnLine 54 (2), 271–277. Tang, C.F., Jiang, R., Wu, Q., Wiwatanapataphee, B., Wu, Y.H., 2007. Mixed traffic flow in anisotropic continuum model. Transp. Res. Rec. 1999 (1), 13–22.
- Tang, C.F., Jiang, R., Wu, Q., Wiwatanapataphee, B., Wu, Y.H., 2007. Mixed traffic flow in anisotropic continuum model. Transp. Res. Rec. 1999 (1), 13–22. Treiber, M., Kesting, A., 2013. Traffic Flow Dynamics: Data, Models and Simulation. Springer.
- Wang, H., Hao, W., So, J., Xiao, X., Chen, Z., Hu, J., 2023. A faster cooperative lane change controller enabled by formulating in spatial domain. IEEE Trans. Intell. Veh.
- Wang, R., Li, Y., Work, D.B., 2017. Comparing traffic state estimators for mixed human and automated traffic flows. Transp. Res. C 78, 95-110.
- Wang, W., Wu, B., 2023. The fundamental diagram of mixed-traffic flow with CACC vehicles and human-driven vehicles. J. Transp. Eng. A Syst. 149 (1), 04022116.
- Yang, H., Jin, W.L., 2014. A control theoretic formulation of green driving strategies based on inter-vehicle communications. Transp. Res. C 41, 48-60.
- Yang, X., Lu, Y., Chang, G.L., 2015. Exploratory analysis of an optimal variable speed control system for a recurrently congested freeway bottleneck. J. Adv. Transp. 49 (2), 195–209.
- Yang, X.-b., Si, B.-f., Huan, M., 2012. Mixed traffic flow modeling near Chinese bus stops and its applications. J. Cent. South Univ. 19 (9), 2697-2704.
- Yao, Z., Hu, R., Wang, Y., Jiang, Y., Ran, B., Chen, Y., 2019. Stability analysis and the fundamental diagram for mixed connected automated and human-driven vehicles. Physica A 533, 121931.
- Yao, Z., Wu, Y., Jiang, Y., Ran, B., 2022. Modeling the fundamental diagram of mixed traffic flow with dedicated lanes for connected automated vehicles. IEEE Trans. Intell. Transp. Syst.
- Yao, Z., Wu, Y., Wang, Y., Zhao, B., Jiang, Y., 2023. Analysis of the impact of maximum platoon size of CAVs on mixed traffic flow: An analytical and simulation method. Transp. Res. C 147, 103989.
- Yuan, Y.M., Jiang, R., Hu, M.B., Wu, Q.S., Wang, R., 2009. Traffic flow characteristics in a mixed traffic system consisting of ACC vehicles and manual vehicles: A hybrid modelling approach. Physica A 388 (12), 2483–2491.
- Yuan, Y., Zhang, Z., Yang, X.T., Zhe, S., 2021. Macroscopic traffic flow modeling with physics regularized Gaussian process: A new insight into machine learning applications in transportation. Transp. Res. B 146, 88–110.
- Zhang, H., Jin, W., 2002. Kinematic wave traffic flow model for mixed traffic. Transp. Res. Rec. 1802 (1), 197-204.
- Zhang, J., Pei, H., Ban, X.J., Li, L., 2022. Analysis of cooperative driving strategies at road network level with macroscopic fundamental diagram. Transp. Res. C 135, 103503.
- Zhang, Z., Yan, X., Wang, H., Ding, C., Xiong, L., Hu, J., 2023. No more road bullying: an integrated behavioral and motion planner with proactive right-of-way acquisition capability. Transp. Res. C 156, 104363.
- Zhang, Y., Zhang, G., Fierro, R., Yang, Y., 2018. Force-driven traffic simulation for a future connected autonomous vehicle-enabled smart transportation system. IEEE Trans. Intell. Transp. Syst. 19 (7), 2221–2233.
- Zhao, H.T., Li, H.Z., Qin, H., Zheng, L.H., 2022. Two-lane mixed traffic flow model considering lane changing. J. Comput. Sci. 61, 101635.
- Zheng, F., Liu, C., Liu, X., Jabari, S.E., Lu, L., 2020. Analyzing the impact of automated vehicles on uncertainty and stability of the mixed traffic flow. Transp. Res. C 112, 203–219.
- Zhou, L., Ruan, T., Ma, K., Dong, C., Wang, H., 2021. Impact of CAV platoon management on traffic flow considering degradation of control mode. Physica A 581, 126193.
- Zhou, J., Zhu, F., 2020. Modeling the fundamental diagram of mixed human-driven and connected automated vehicles. Transp. Res. C 115, 102614.
- Zhu, W.X., Zhang, H.M., 2018. Analysis of mixed traffic flow with human-driving and autonomous cars based on car-following model. Physica A 496, 274–285.